DEUTSCHES ELEKTRONEN-SYNCHROTRON DESY

DESY 76/42
August 1976

Electroproduction of Baryon Resonances

by

Jörg Gayler
Deutsches Elektronen-Synchrotron DESY, Hamburg

Abstract:

Data on inelastic electroproduction below W = 2 GeV are reviewed. It is reported on total cross section measurements, threshold experiments and the data of π^+, π^o and η production.
The latest data at $q^2 \simeq 1$ GeV^2 are analysed with the technique of Devenish and Lyth.

2 HAMBURG 52 · NOTKESTIEG 1

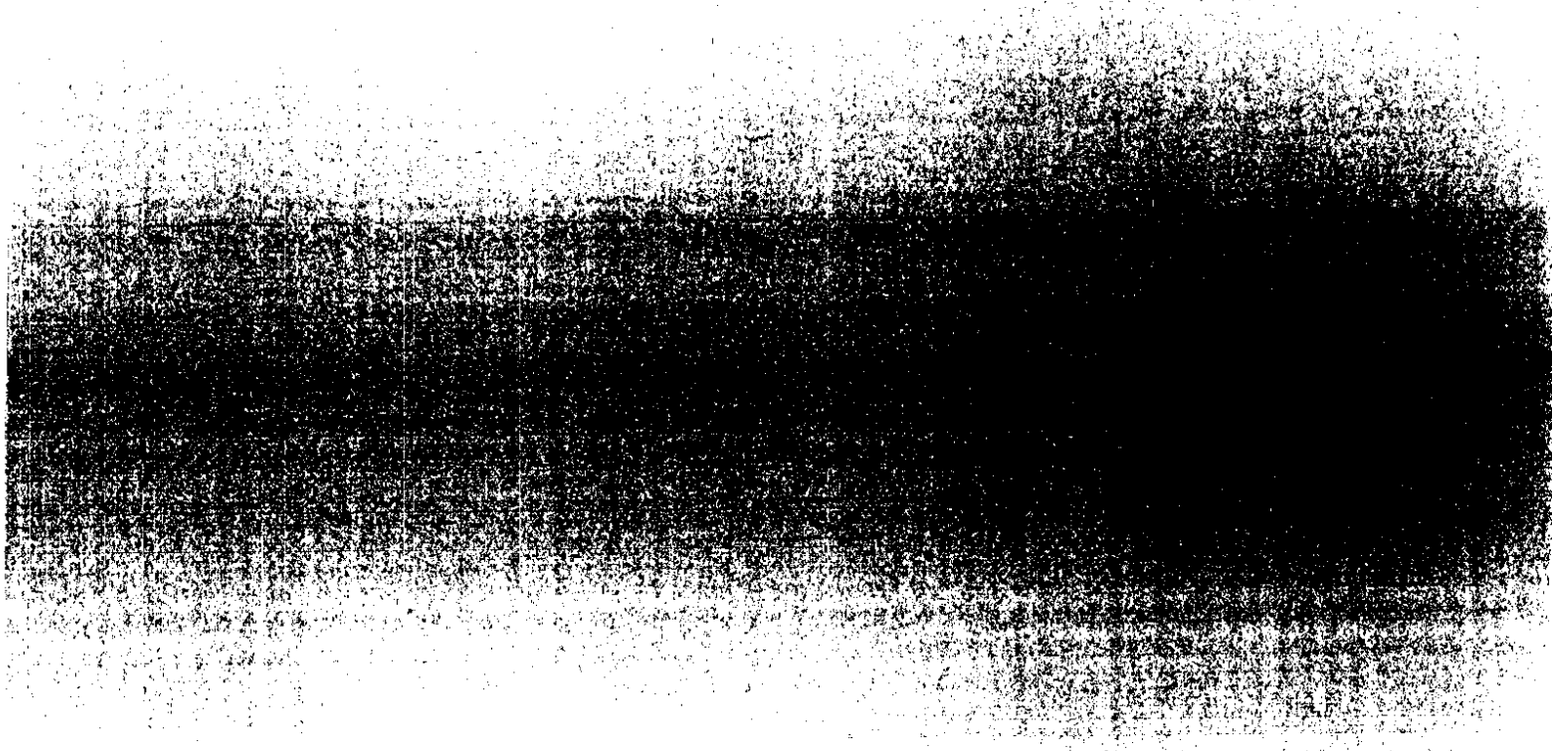

To be sure that your preprints are promptly included in the
HIGH ENERGY PHYSICS INDEX ,
send them to the following address (if possible by air mail) :

DESY
Bibliothek
2 Hamburg 52
Notkestieg 1
Germany

Electroproduction of Baryon Resonances

Jörg Gayler

Deutsches Elektronen-Synchrotron DESY, HAMBURG

Abstract

Data on inelastic electroproduction below W = 2 GeV are reviewed. It is reported on total cross section measurements, threshold experiments and the data of π^+, π^o and η production. The latest data at $q^2 \simeq 1$ GeV^2 are analysed with the technique of Devenish and Lyth.

Invited talk given at the Topical Conference on Baryon Resonances, July 5-9, 1976, Oxford, England

1. Introduction

The main purpose of this paper is to give some picture of the experimental information available from electron nucleon scattering in the resonance region.

This field of physics is still very interesting in spite of all the new and exciting descoveries of the last years. These electroproduction experiments are on one side very close to photoproduction, where the excitation of baryon resonances is described with some success by transitions between bound 3 quark states. These models can be tested more severely by electroproduction. On the other side electron scattering in the resonance region is in intimate connection (Bloom Gilman duality[1]) to deep inelastic phenomena, where again quark concepts are very successful.

In this report I will not repeat everything in detail, that has been discussed in ref. 2, but spend some more time on information that became available since April 1975.
In section 2 the notation will be clarified. In section 3 the total cross section experiments will be reviewed. Sections 4 and 5 are devoted to electroproduction experiments, where the final state is observed. Threshold experiments will be shortly discussed (section 4), which aim to determine the axial vector nucleon form factor. In some detail we will discuss the latest experiments on π^o, π^+ and η production in the second and third resonance region. This will be done by a multipole analysis using the technique of Devenish and Lyth[3].

2. Kinematics

We assume that one photon exchange is adequate for describing eN scattering (fig. 1). An electron of energy E hits a nucleon of mass M at rest in the laboratory. Detection of the secondary electron with energy E' and scattering angle ϑ defines the momentum transfer

$$q^2 = 4EE' \sin^2 \vartheta/2$$

the secondary hadronic mass

$$W^2 = s = M^2 + 2M\nu - q^2,$$

with $\nu = E - E' = P_N\, q/M$.

The scaling variables ω, ω' are given by

$$\omega = 2M\nu/q^2$$
$$\omega' = (2M\nu + M^2) \,/\, q^2 = W^2/q^2 + 1.$$

The single arm cross section can be written in terms of the structure functions $W_1(\nu,q^2)$, $W_2(\nu,q^2)$:

$$\frac{d^2\sigma}{d\Omega\, dE'} = 4\alpha^2 \frac{E'^2}{(q^2)^2} \left[2W_1 \sin^2 \vartheta/2 + W_2 \cos^2 \vartheta/2\right]$$

or in terms of the transverse and longitudinal virtual photoproduction total cross sections

$$\frac{d^2\sigma}{d\Omega\, dE'} = \Gamma_t \,(\sigma_t + \varepsilon\sigma_\ell)$$

with the "flux factor" Γ_t given by

$$\Gamma_t = (\alpha/2\pi^2)\, E'/E\, (K/q)\, \frac{1}{1-\varepsilon},$$
$$K = \frac{W^2 - M^2}{2M}.$$

The transverse polarization ε of the virtual photon is given by

$$\varepsilon = (1 + 2 \tan^2 \vartheta/2 \,(1 + \frac{\nu^2}{q^2}))^{-1}.$$

If the coincidence cross section is expressed as differential virtual photon absorption cross section in the hadronic centre of mass system (CMS), we obtain[4]:

$$\frac{d\sigma}{d\Omega^*} = \frac{1}{\Gamma_t} \frac{d\sigma}{d\Omega\, dE'\, d\Omega^*}$$

$$\frac{d\sigma}{d\Omega^*} = \sigma_U + \varepsilon\sigma_L + \sigma_P \sin^2\theta^* \cos 2\phi + \sqrt{2\varepsilon(\varepsilon+1)}\, \sigma_I \sin\theta^* \cos\phi. \qquad (1)$$

The angle θ^* is the polar production angle measured versus the virtual γ ray in the CMS, ϕ is the azimuth (fig. 1).
The σ-terms represent cross sections for unpolarized photons (σ_U) and for longitudinal (or scalar) photons (σ_L), a transverse polarization term (σ_P) and a longitudinal-transverse interference term (σ_I).

These terms may be further decomposed in multipole or in helicity amplitudes[5]. Usually one distinguishes the transverse multipoles $M_{\ell\pm}$ (magnetic) and $E_{\ell\pm}$ (electric) and scalar multipoles $S_{\ell\pm}$ (or equivalently longitudinally multipoles $L_{\ell\pm}$). The subscript $\ell_\pm$ refers to the spin of the hadronic system which is given by $j = \ell \pm 1/2$ where ℓ is the mesons angular momentum. A transverse multipole is magnetic (electric) if the total angular momentum absorbed from the virtual γ-field is ℓ ($\ell \pm 1$). Instead of multipoles, helicity partial wave amplitudes $A_{\ell\pm}$, $B_{\ell\pm}$ and $C_{\ell\pm}$ may be used. The absolute value of the total helicity of the ingoing γ and nucleon can take the values 1/2 (A-amplitude), 3/2 (B-amplitude) in case of transverse photons and 1/2 (C-amplitude) in case of scalar photons. The subscripts $\ell_\pm$ are defined as above.
$C_{\ell\pm}$ is scalar therefore $C_{\ell\pm} \sim S_{\ell\pm}$. The transverse multipoles are related to the transverse helicity elements as follows[5]:

$$A_{\ell+} = \frac{1}{2}\left(\ell M_{\ell+} + (\ell+2)\, E_{\ell+}\right)$$

$$A_{\ell+1,-} = \frac{1}{2}\left((\ell+2) M_{\ell+1,-} - \ell E_{\ell+1,-}\right)$$

$$B_{\ell+1,+} = -M_{\ell+1,+} + E_{\ell+1,+}$$

$$B_{\ell+2,-} = M_{\ell+2,-} + E_{\ell+2,-} \qquad ,\ell = 0,1,\ldots$$

The normalization of the multipoles used in section 5 is that of CGLN[6] and e.g. v. Gehlen[7].

As the experimental data available are generally not sufficient to allow for an unambiguous multipole expansion, the measured angular distributions are often expressed in terms of angular coefficients. If we assume that only s, p and d-waves with total angular momentum $j \leq \frac{3}{2}$ contribute to the final πN state, the cross section can be written as follows (c.f. e.g. ref. 8):

$$\begin{aligned} \sigma_U + \varepsilon\sigma_L &= \bar{A}_o + \bar{A}_1 \cos\theta^* + \bar{A}_2 \cos^2\theta^* + \bar{A}_3 \cos^3\theta^* \\ \sigma_P &= (C_o + C_1 \cos\theta^*) \sin^2\theta^* \\ \sigma_I &= (D_o + D_1 \cos\theta^* + D_2 \cos^2\theta^*) \sin\theta^* \end{aligned} \qquad (2)$$

If we allow in addition for F waves with $j = 5/2$ the following 3 terms $\bar{A}_4 \cos^4\theta^*$, $C_2 \cos^2\theta^* \sin^2\theta^*$, $D_3 \cos^3\theta^* \sin\theta^*$ have to be added. The total virtual photoproduction cross section is then given by:

$$\sigma_{tot} = 4\pi\left(\bar{A}_o + \frac{1}{3}\bar{A}_2 + \frac{1}{5}\bar{A}_4\right) \qquad (3)$$

3. Total Cross Section Measurements

Progress in the field of total cross section measurements, where only the scattered electron is detected, is nowadays very slow in the resonance region. This is due to the facts that first, a large amount of information is avialable already and second, it is a difficult and a tedious task to measure something, which is really new. New information would be data at momentum transfers $q^2 \approx 6$ GeV^2 or precise measurements on $R = \sigma_\ell/\sigma_t$. Both implies measurements of very small cross sections.

There has been performed a new experiment at the Bonn Synchrotron where the total ep cross section in the first and second resonance region has been measured at large scattering angles (around 70°) with small polarization $\varepsilon \approx 0.25$ of the virtual photon[9]. The apparatus is shown in fig.2. The cross sections agree with other measurements at large ε(see fig. 3).

In a recent analysis[10], which is a repetition of older work with less data[11], the world data of ep scattering in the resonance region have been compiled and fitted separately in bins of W and ε according an empirical Ansatz for the q^2-dependence. As an example the resulting cross sections at $q^2 = 1$ GeV^2 of the fits, using data with $\varepsilon \geq 0.9$, are compared to those with $\varepsilon \leq 0.6$ in fig. 4. On average $\Delta\varepsilon \approx 0.5$ for the two data sets. The difference

$$\sigma_{\varepsilon \geq 0.9} - \sigma_{\varepsilon \leq 0.6} \approx \frac{1}{2}\sigma_\ell$$

indicates that σ_ℓ is essentially zero in the second resonance region, but might be of the order of 10 % to 20 % in the third resonance region.

A survey of the total γ_v p cross sections in the resonance region is given in fig. 5.

The following facts are obvious:

a) The first resonance $\Delta(1232)$ is very prominent at small momentum transfers but hardly visible at $q^2 = 6$ GeV^2.
b) The second resonance peak stays equally prominent at all momentum transfers.
c) The third peak considerably moves in position with increasing q^2.

We inspect this in somewhat more detail: in fig. 6 the spectrum at $q^2 = 0.1$ GeV^2 has been normalized at the peak of the second resonance to the spectrum at $q^2 = 3$ GeV^2.
At large momentum transfers there is some kind of plateau developing between the first and the second resonance peak, not yet visible at $q^2 = 0.1$ GeV^2. The second peak is more narrow at $q^2 = 3$ GeV^2 and slightly more prominent. The change is more distinctly visible at the low energy side and may be due to the resonance $S_{11}(1535)$ which mainly decays into ηp, and increases in relative importance with increasing momentum transfer (see section 5.2). A drastic change in the third resonance region is visible. If the third peak is treated as one resonance and described by a Breit Wigner function as done most recently by Stein et al. the peak position moves from $W_R = (1675 \pm 3.1)$ MeV at $q^2 = 0.08$ GeV^2 to $W_R = (1713 \pm 1.4)$ MeV at $q^2 = 1.75$ GeV^2 [12]. It seems questionable whether the third peak is still dominated by the resonance $F_{15}(1688)$ at high momentum transfers as in photoproduction.

The q^2-dependence, according the fits of ref. 10, is plotted in fig. 7a in the case of 5 values of W (W = 1.215, 1.4, 1.5, 1.7 and 1.9 GeV). Up to $q^2 = 6$ GeV^2 the cross section at W = 1.215 GeV, which is a sum of the $\Delta(1232)$ and nonresonant background, has the fastest decrease with q^2.
The q^2-dependence of the background is quite different:
The cross section at W = 1.4 GeV, which to a large part is given by background, has at high momentum transfers the slowest decrease with increasing q^2. This is more distinctly visible in fig. 7b, where the 5 chosen cross sections have been normalized to the ρ propagator squared.

The cross section at W = 1.4 GeV is nearly proportional to $1/(m_\rho^2+q^2)^2$ at $q^2 > 1$ GeV^2. With the exception of W = 1.4 GeV, fig. 7b, reflects the general behaviour, that the larger the value of W, the larger the momentum transfer q^2 needed at which the cross section begins to decrease faster than $1/(m_\rho^2+q^2)^2$. This corresponds to the fact, that the resonances average the universal scaling curve of deep inelastic ep scattering and slide it down versus $\omega = 1$ with increasing q^2, as first discussed by Bloom and Gilman [1].

For further information on single arm measurements in the resonance region, I refer to the work of Stein et al. [12], Köbberling et al. [13] and ref. 2.

4. Threshold Electroproduction and the axial Vector Form Factor of the Nucleon

Since several years there has been considerable effort, both experimental and theoretical, to determine the axial vector form factor of the nucleon $g_A(q^2)$ from electroproduction data.
The s-wave threshold cross section of the reaction

$$ep \to e'n\pi^+$$

can be related in the soft pion limit ($m_\pi = 0$, i.e. zero four momentum at threshold) to the form factor $g_A(q^2)$. These calculations involve current algebra and PCAC. It is therefore very interesting to compare the results of electroproduction with the more directly determined results on $g_A(q^2)$ from the reaction $\nu n \to \mu^- p$ (the latter are obtained assuming CVC and absence of second class currents).

On the other hand these comparisons are by no means straight forward. The separation of s-wave threshold π^+ production from resonant p-wave production and the extrapolation to the soft pion limit has been performed with the help of model calculations of pion production. Therefore a comparison of the resulting axial vector form factors from electron and neutrino-scattering only tests several theoretical principles and detailed model calculations together.

In addition to single arm experiments [14] there have been 3 experiments where the secondary electron and neutron have been detected in coincidence. The Frascati experiment [15] measures the total cross section of $ep \to e'\pi^+n$, whereas at DESY [16] and Daresbury [17] also the angular distribution has been analysed.

The Daresbury-Pisa experiment has been extended to higher momentum transfer (up to $q^2 = 0.88$ GeV^2) [49]. An evaluation of the available coincidence threshold data on $ep \to e\pi^+n$ (fig. 9a) gives an excellent fit by the dipole formula

$$\frac{g_A(q^2)}{g_A(0)} = \frac{1}{(1+q^2/m_A^2)^2}$$

with the result of $m_A = 0.96 \pm 0.03$ GeV. The form factors have been evaluated by the model of Benfatto, Nicolo and Rossi [50].

Recently the reaction

$$ep \to e'\pi^- \Delta^{++}$$

has been investigated by a DESY-Glasgow-collaboration, which gives an interesting and to some extent independent determination of $g_A(q^2)$[18]. The experiment is rather clean: all 4 final state particles are detected in a streamer chamber. Furthermore the relevant matrix element (the contact term)

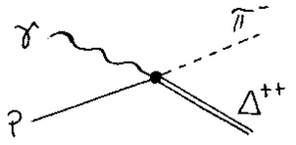

seems to dominate the cross section[19], whereas it might be more difficult to get rid of the p-wave contribution at the reaction $ep \to e'\pi^+ n$. Fig. 8 shows the strong rise of the $\pi^- \Delta^{++}$ total cross section at an average momentum transfer $\langle q^2 \rangle = 0.6$ GeV^2. The observed rise above threshold and the flatness of the π^- CMS angular distribution supports the interpretation as s-wave production[19].
Fig. 9b shows the q^2-dependence, in comparison to 1 over the ρ propagator squared.

These authors evaluated $g_A(q^2)/(g_A(0)$ by comparison with a calculation of Adler and Weisberger[51]. In fig. 9c they compare their results with data on $ep \to e\pi^+ n$, which are in this case evaluated by the model of Dombey and Read[52]. The agreement of these different experiments is encouraging. A dipoe fit to the data in fig. 9c results in $m_A = 1.16 \pm 0.03$ GeV[18].
The corresponding result from ν scattering is $m_A = 0.89 \pm 0.08$ GeV[20], which is close to the result obtained by A. del Guerra et al.[49] using the model of Benfatto, Nicolo and Rossi.

5. Electroporduction of π^0, π^+ and η Mesons

5.1 Region of the $\Delta(1232)$

An experiment on π^+ production has been performed recently at Saclay by G. Bardin et al.[21]. The differential cross section of π^+ mesons produced in the direction of the virtual photon ($\theta^*_{\pi^+} = 0^\circ$) has been measured at W = 1.175 GeV and $q^2 = 1$ fm$^{-2} = 0.039$ GeV^2 at $\varepsilon = 0.65$ and at $\varepsilon = 0.2$. The longitudinal cross section is found to be about twice as large as the

transverse one ($R \simeq 2$). This should be a measure of the pion exchange graph

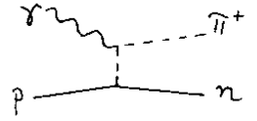

which is purely longitudinal in the forward direction due to angular momentum conservation.
The experimental situation of π^0 production at the first resonance is essentially unchanged since 1972. There exist reviews on the subject (e.g. refs. 22,23). I recall the main facts of π^0 electroproduction experiments[24 to 27] and add some further remarks.

a) The magnetic dipole M_{1+} dominates the cross sections as expected by the quark model up to $q^2 = 1.6$ GeV^2. There are no coincidence data at higher momentum transfers.
b) There is some scalar excitation of the resonance
$|S_{1+}|/|M_{1+}| \sim 5\ \% \ldots 10\ \%$.
c) E_{1+} is small at resonance
$|E_{1+}|/|M_{1+}| < 5\ \%$
d) SP-wave interference is observed.
e) The transition form factor $G^*_M(q^2)$ which has been extracted from the data, shows approximately dipole behaviour, but decreases more rapidly with increasing q^2 than the nucleon form factor $G_M(q^2)$.
f) The available dispersion theoretical models[3,7] do not describe satisfactortily the tail of the $\Delta(1232)$ at $q^2 \gtrsim 1$ GeV^2.

The results on $G^*_M(q^2)$ from total cross section data are rather uncertain at $q^2 \gtrsim 2$ GeV^2 as the resonance gets less prominent with increasing momentum transfer (see fig. 5). The situation has been reviewed in more detail in ref. 2. The theoretical ambiguities involved in the comparison of N and NΔ transition form factors have been discussed recently by Devenish, Eisenschitz and Körner[28].

From duality to deep inelastic processes one would expect total helicity 1/2 in the γ_v N-system to dominate at large momentum transfers. If so, two possibilities are immediately at hand: Either the electric excitation of the Δ will be important at large momentum transfers (cf.

also ref. 29)) or the Δ excitation stays magnetic as expected by the simple picture of a quark spin flip, but gets irrelevant compared to a background which is produced mainly by helicity 1/2 in the γ_v N system.
There is an experiment in progress at DESY at $q^2 = 3$ GeV^2, which will shed some light on these questions.

5.2 Electroproduction of η Mesons in the Region of $S_{11}(1535)$

Progress in the understanding of the second resonance region was strongly favoured during the last years due to the lucky circumstance that the resonance $S_{11}(1535)$ has a large branching ratio ($\simeq 0.65$) to the decay channel ηp. There are data from three experiments[30,31,32] on η production, all of them use the missing mass technique to identify the final state ηp (fig. 1o). The observed W-dependence[32] and the flatness of the decay angular distribution in the CMS of the final hadrons strongly supports the interpretation, that the observed η production is due to the resonance $S_{11}(1535)$.

A considerable contribution of $P_{11}(147o)$ ($\Gamma_{\eta N}/\Gamma_{total} \simeq 0.18$[33]) should show up in the data by interference with $S_{11}(1535)$ as strong forward backward asymmetry, which is not observed.

The second resonance peak, which is essentially a sum of $S_{11}(1535)$ and $D_{13}(1525)$ stays equally prominent at all momentum transfers (fig. 5). It is therefore concluded from the results on the total cross section of $\gamma_v p \to \eta p$ in comparison with $\gamma_v p \to X$ (fig. 11), that contrary to $S_{11}(1535)$ the $D_{13}(1525)$ falls much faster with increasing q^2 than the total ep cross section. But the present data do not allow any conclusion whether this behaviour continues at $q^2 \geq 1$ GeV^2. It might well be the case, that the N-N* transition form factors of the two resonances, which are members of a $SU_6(^{1/2}8, 70, L=1^-)$ multiplet, are asymptotically proportional. Further information on this question is to be expected from forthcoming experiments at Daresbury and DESY at $q^2 = 2$ and 3 GeV^2.

The possibility of scalar excitation is investigated by an experiment at DESY. A missing mass distribution taken at $\varepsilon = 0.5$ (fig. 12) shows a strong η signal indicating that the scalar cross section is small.

5.3 π^o and π^+ Electroproduction above the first Resonance Region

It is a well known fact, that photoproduction of the resonances $D_{13}(152o)$ and $F_{15}(1688)$ proceeds dominantly in the helicity $\frac{3}{2}$ state of the ingoing γp system, as predicted by quark model calculations[34]. That

this is different at space like momentum transfers is to be expected from the detailed quark models, but also from duality to deep inelastic scattering, where helicity $\frac{1}{2}$ is expected do dominate from quark parton models. And indeed a positive helicity asymmetry

$$A = (\sigma_{1/2} - \sigma_{3/2}) \; / \; (\sigma_{1/2} + \sigma_{3/2})$$

where $\sigma_{1/2}$ and $\sigma_{3/2}$ are the total cross section for excitation with helicity 1/2 and 3/2 respectively has been measured recently in the inelastic continuum using a polarized electron beam and a polarized target at SLAC[35].

The first data to demonstrate the importance of helicity 1/2 excitation in the resonance region, were the forward π^+ data from Evangelides et al.[36] (fig. 13) which distinctly show resonant structure. (Helicity 3/2 can not contribute to the forward and backward directions.) This was confirmed by data at $q^2 = 0.6$ and 1 GeV^2 from DESY in the case of π^+ forward[37] and π^o backward production[38] (fig. 13, 14).

The close relationship between resonance production and deep inelastic phenomena has recently been demonstrated in a different way by A. Browman et al.[4o]. The W-dependence of single π^+ production at large angles has been measured at $q^2 = 1.2$ GeV^2 (fig. 15). The W-dependence observed at $\theta^*_{\pi^+} = 90^o$ agrees with the prediction of a parton intercharge model[41]. In the present context it is interesting to note that the fall of the cross section is continued into the resonance region.

The changing helicity structure in the second resonance region is hardly to be recognized from the π^o angular distributions. Similar to photoproduction the cross section is large around $\theta^*_{\pi^o} = 90^o$ and small in the forward and backward directions (see figs. 16, 17 and 18).
The π^o angular distributions of ref. 38 have been analyzed in terms of the angular coefficients defined in eq. 2 (section 2). The results of the most important coefficients $\bar{A}_o$, $\bar{A}_2$, C_o are shown in fig. 19. A pure helicity 3/2 excitation of the resonance $D_{13}(152o)$ would contribute $\bar{A}_2 = -\bar{A}_o$, $C_o = 0$. And again, the data are very close to that. But the data are consistent with considerable helicity 1/2 excitation if the strong contribution of the resonance $S_{11}(1535)$ to the observed structure is taken into account.

The authors of refs. 38, 39 used the results on the angular coefficients to estimate the total cross section of π^o production (fig. 2o).

The results of ref. 38 at $q^2 = 0.6$ GeV^2 have been improved by a more careful analysis by M. Merkwitz[42].
Some examples of π^+ angular distributions are given in figs. 21, 22.

5.4 Analysis with the Technique of Devenish and Lyth

Some of the important experimental results of electroproduction in the resonance region have been made visible only by the multipole analysis of Devenish and Lyth[3] (DL hereafter). DL had used the ep → πN data available at the end of the year 1974. In addition data on the resonance peak heights as determined by Breit Wigner fits[13,44] to ep → eX data and the total cross section of $S_{11}(1535)$ as measured by η production had been used.
In the analysis of DL the resonance region is built up out of 11 resonances, which appeared to be important in photoproduction[45]. The q^2-dependence of the form factors is parametrized consistently with their known threshold behaviour.
With these form factors and Breit-Wigner's DL compute the imaginary parts of the amplitudes and couple these with the real parts by fixed t-dispersion relations. The form factor parameters are then determined by fits to the data and required continuity to the results of photoproduction[45].

It was desirable to repeat part of the analysis of DL because only a preliminary subset of the data sample from DESY[37,38] had been available to DL.
To avoid uncertainties and possibly unnecessary constraints due to the parametrization not all data are treated together in the present analysis, but it is tried to find a solution for one q^2 value only*. A rather complete set of coincidence data now exists at $q^2 \approx 1$ GeV^2. Therefore only differential cross sections as listed in refs. 37 and 42 together with $S_{11}(1535)$ results from η production[30,32] and resonance peak height data[12,13,44], all at $q^2 \approx 1$ GeV^2 are used. (The procedure of fitting corresponds to the "standard fit" of DL[3], only the relative weights of S_{11} and peak height data compared to πN data are reduced to 0.2 and 0.1 respectively.)

* This was suggested by A.J.G. Hey

The multipole amplitudes thus obtained (hereafter referred to as fit 1) reproduce the general behaviour of the data, but not all the details. The average χ^2 per data point is 3.2, which is comparable with or better than the results of photoproduction[45]. Examples of angular distributions of π^0 and π^+ production are given in figs. 17 and 21. The deviations are more significant in the separated cross section data (fig. 18 and 22). The main shortcomings are the following:

a) the cross sections are too low at small energies ($W \leq 1.415$ GeV).
b) The forward π^+ and backward π^0 production cross sections are only very roughly reproduced (figs. 13 and 14).

The main results of fit 1 are the following:

1a) There is no indication of a scalar excitation of the second resonance peak. (DL[3] found considerable scalar excitation of $S_{11}(1535)$.)
1b) The third resonance peak has a scalar contribution of about 5 %.
1c) $P_{11}(1470)$ improves the fit considerably. But there is no clear signal of its presence.
As the fits are unsatisfactory between the first and second resonance region, no clear statement about the presence or absence of $P_{11}(1470)$ can be made.
1d) The excitation of $D_{13}(1520)$ is purely magnetic (see fig. 23). This leads to a ratio $A_{2-}/B_{2-} \approx 1.5$, which is clearly above the results of DL[3] (fig. 24).
1e) At $F_{15}(1688)$ we obtain $M_{3-} \approx 2E_{3-}$, $A_{2-}/B_{3-} \approx 1.0$ (figs. 23,24).

What kind of solutions would better reproduce the experimentally observed π^+ forward and π^0 backward structure?
To answer this question, a second fit (fit 2) was tried, where besides the peak height and $S_{11}(1535)$ data only the forward π^+ and backward π^0 data were used.
The main results of fit 2 are as follows:

2a) The second resonance peak has some scalar part from $S_{11}(1535)$. The latter has a ratio of scalar to transverse excitation of about 18 % (about 11 % at DL[3]).
2b) The third resonance peak has a scalar contribution of ~ 6 % (similar to 1b)

2c) There is no indication of $P_{11}(1470)$ in agreement with DL.

2d) At $D_{13}(1520)$ we obtain $M_{2-} \simeq 2E_{2-}$, $A_{2-}/B_{2-} \simeq 0.8$, close to the results of DL (figs. 23, 24).

2e) The excitation of $F_{15}(1688)$ is dominantly magnetic. The resulting helicity ratio $A_{3-}/B_{3-} \approx 1.6$ is above the results of DL (fig. 24).

The influence of the uncertainties in the region of $P_{11}(1470)$ on the helicity ratios A_{2-}/B_{2-} and A_{3-}/B_{3-} can be estimated from a fit of type I where the parameters of $P_{11}(1470)$ have been fixed to the results of fit 2. The results obtained are $A_{2-}/B_{2-} \simeq 1.2$ (1.5 at fit 1) and $A_{3-}/B_{3-} \approx 0.75$ (≈ 1.0 at fit 1).

The results are compared in terms of the helicity asymmetry, defined above, in fig. 25 with quark model predictions of Ravndal[46] and and Ono[47], and with a model of Körner et al.[48], who compute the helicity structure of s-channel resonances by duality from SU_3 t-channel constraints.

Conclusions:

a) Rather stable results are found for the resonances $S_{11}(1535)$, $D_{13}(1520)$ and $F_{15}(1688)$ (besides $P_{33}(1232)$.

b) The helicity structure of $D_{13}(1520)$ and $F_{15}(1688)$ change rapidly with q^2, probably more rapidly than according the results of DL[3].

c) The electric multipoles of both resonances fall much faster with q^2 than the magnetic ones.

d) The present analysis can not probe the absence of $P_{11}(1470)$ in electroproduction at $q^2 \approx 1$ GeV^2 (nor its presence).

d) Further improvements of the multipole analysis especially in the region of the tail of $P_{33}(1232)$ are desirable.

Acknowledgements:

I want to thank R.C.E. Devenish for patiently introducing me into his programs and for very helpful discussions. I am grateful to Mrs. Schmöger for her help with the manuscript.

References

1. E.D. Bloom, E.J. Gilman, Phys. Rev. D4 (1971) 2901

2. J. Gayler, Proceedings of the 8th Session of Spring School of Experimental and Theoretical Physics, Yerevan, 1975

3. R.C.E. Devenish, D.H. Lyth, Nucl. Phys. B93 (1975) 109

4. C.W. Akerlof, W.W. Ash, K. Berkelman, M. Tigner, Phys. Rev. Letters 14 (1965) 1036

5. H.F. Jones, Il Nuovo Cimento, 40 (1965) 1018

6. C.F. Chew, M.L. Goldberger, F.E. Low, Y. Nambu, Phys. Rev. 106 (1957) 1345

7. G. v. Gehlen, Nucl. Phys. B20 (1970) 102

8. W.J. Shuttleworth, A. Sofair, R. Siddle, B. Dickinson, M. Ibbotson, R. Lawson, H.E. Montgomery, R.D. Hellings, J. Allison, A.B. Clegg, F. Foster, G. Hughes, P.S. Kummer, Nucl. Phys. B45 (1972) 428

9. V. Burkert, Bonn-IR-75-27, Bonn University, 1975

10. F.W.Brasse, W. Flauger, J. Gayler, S.P. Goel, R. Haidan, M. Merkwitz, H. Wriedt, DESY 76/11 (1976) and Nucl. Phys. B (to be published)

11. F.W. Brasse et al., DESY 71/2 (1971)

12. S. Stein et al., Phys. Rev. D12 (1975) 1884

13. M. Köbberling et al., Nucl. Phys. B82 (1974) 201

14. V.P.R. Nuthakki et al., Nucl. Phys. B31 (1971) 360

Yu. I. Titov et al., Phys. Letters 37B (1971) 422

E.D. Bloom et al., Phys. Rev. Letters 30 (1973) 1186

15. E. Amaldi, M. Benventano, B. Borgia, F. De Notaristefani, A. Frondaroli, P. Pistelli, I. Sestili, M. Severi, Phys. Letters 41B (1972) 216

16. P. Brauel, F.-W. Büsser, Th. Canzler, D. Cords, W.R. Dix, R. Felst, G. Grindhammer, W.-D. Kollmann, H. Krehbiel, J. Meyer, G. Weber, Phys. Letters 45B (1973) 389

17. A. del Guerra, A. Giazotto, M.A. Giorgi, A. Stefanini, D.R. Botterill, D.W. Braben, D. Clarke, P.R. Norton. Nucl. Phys. B99 (1975) 253

18. P. Joos, A. Ladage, H. Meyer, P. Söding, P. Stein, G. Wolf, S. Yellin, C.K. Chen, J. Knowles, D. Martin, H.M. Scarr, I.O. Skillicorn, K. Smith, C. Benz, G. Drews, D. Hoffmann, J. Knobloch, W. Kraus, H. Nagel, E. Rabe, C. Sander, W.-D. Schlatter, H. Spitzer and K. Wacker, DESY 76/09 (1976)

19. P. Joos et al., Phys. Letters 52B (1974) 48

2o. D.H. Parkins, Proceedings of the 1975 International Symposium on Lepton and Photon Interactions in Stanford, p. 571

21. G. Bardin, J. Duclos, J. Julien, A. Magnon, Lettre al Nuovo Cimento, 13 (1975) 485

22. R. Wilson, Proceedings of the 1971 International Symposium on Electron and Photon Interactions at High Energies, edited by N.B. Mistry (Cornell University), 1972

23. J. Gayler in Daresbury Study Weekend on Inelastic Electron Scattering (1971), DNPL/R15 edited by A. Donnachie

24. W. Albrecht et al., Nucl. Phys. B25 (197o)1

25. R. Siddle et al., Nucl. Phys. B35 (1971) 93

26. J.-C. Alder et al., Nucl. Phys. B46 (1972) 573

27. K. Bätzner et al., Nucl. Phys. B76 (1974) 1

28. R.C.E. Devenish, T.S. Eisenschitz, J.G. Körner, DESY 75/48 (1975)

29. B.L. Ioffe, Preprint ITEP 50 (1976)

3o. P.S. Kummer, E. Ashburner, F. Foster, G. Hughes, R. Siddle, J. Allison, B. Dickinson, E. Evangelides, M. Ibbotson, R.S. Lawson, R.S. Meaburn, H.E. Montgomery, W.J. Shuttleworth, Phys. Rev. Letters 30 (1973) 873

31. U. Beck, K.H. Becks, V. Burkert, J. Drees, B. Dresbach, B. Gerhardt, G. Knop, H. Kolanoski, M. Leenen, K. Moser, H. Müller, C.H. Nietzel, J. Päsler, K. Rith, M. Rosenberg, R. Sauerwein, E. Schlösser, H.E. Stier, Physics Letters 51B (1974) 1o3

32. J.-C. Alder, F.W. Brasse, W. Fehrenbach, J. Gayler, R. Haidan, G. Glöe, S.P. Goel, V. Korbel, W. Krechlok, J. May, M. Merkwitz, R. Schmitz, W. Wagner, Nucl. Phys. B91 (1975) 386

33. Particle Data Group, Rev. Mod. Phys. 48 (1976)

34. L.A. Copley, G. Karl, E. Obryk, Nucl. Phys. B13 (1969) 3o3

35. K. Schüler, talk presented at the Frühjahrstagung of DPG, Karlsruhe (1976)

36. E. Evangelides, R. Meaburn, J. Allison, B. Dickinson, M. Ibbotson, R. Lawson, H.E. Montgomery, D. Baxter, F. Foster, G. Hughes, P.S. Kummer, D.H. Lyth, R. Siddle, R.C.E. Devenish, Nucl. Phys. B71 (1974) 381

37. J.-C. Alder, H. Behrens, F.W. Brasse, W. Fehrenbach, J. Gayler, S.P. Goel, R. Haidan, V. Korbel, J. May, M. Merkwitz, Nucl. Phys. B99 (1975), 1, DESY 75/29 (1975)

38. J.-C. Alder et al., Nucl. Phys. B1o5 (1976) 253

39. W.J. Shuttleworth, A. Sofair, R. Siddle, B. Dickinson, M. Ibbotson, R. Lawson, H.E. Montgomery, R.D. Hellings, J. Allison, A.B. Clegg, F. Foster, G. Hughes and P.S. Kummer, Nucl. Phys. B45 (1972) 428

4o. A. Browman, K.M. Hanson, S.D. Holmes, R.V. Kline, D. Larson, F.M. Pipkin, S.W. Raither, A. Silverman, Phys. Rev. Letters 35 (1975) 1313

41. S.J. Brodsky, G.R. Farrar, Phys. Rev. Lett. 31, 1153 (1973)

42. M. Merkwitz, DESY Internal report F21-76/01 (1976)

43. J. Gayler, DESY Internal Report F21-71/2 (1971)
J. May, DESY Internal Report F21-71/3 (1971)

44. M. Breidenbach, Thesis, MIT Report No. 2o98-635 (197o)

45. R.C.E. Devenish, D.H. Lyth, W.A. Rankin, Phys. Rev. Letters 52B (1974) 227

46. F. Ravndal, Phys. Rev. D4 (1971) 1466

47. S. Ono, Preprint, Technische Hochschule Aachen (1976)

48. J.G. Körner, I. Bender, A. Actor, DESY 75/57 (1975)

49. A. del Guerra, A. Giazotto, M.A. Giorgi, A. Stefanini, D.R. Botterill, H.E. Montgomery, P.R. Norton, G. Matone, Daresbury Report DL/P 256

5o. G. Benfatto, F. Nicolo, G.C. Rossi, Nucl. Phys. B50 (1972) 2o5 and Nuovo Cimento 14A (1973) 425

51. S.L. Adler, W.I. Weisberger, Phys. Rev. 169, 1392 (1968)

52. N. Dombey, B.J. Read, Nucl. Phys. B6o (1973) 65
B.J. Read, Nucl. Phys. B74 (1974) 482

Figure Captions

Fig. 1: One photon exchange diagram, definition of angles.

Fig. 2: Apparatus of V. Burkert et al. to measure $\sigma_t + \varepsilon\sigma_\ell$ at $\varepsilon \simeq 0.25$ (from Ref. 9).

Fig. 3: Total cross sections measured at Bonn with $\varepsilon \simeq 0.25$ in comparison with other data (from ref. 9).

Fig. 4: $\sigma_t + \varepsilon\sigma_\ell$ at $q^2 = 1$ GeV^2 as determined by fits on data with $\varepsilon \geq 0.9$ (O) and on data with $\varepsilon \leq 0.6$ (Δ)(from ref. 1o).

Fig. 5: $\sigma_t + \varepsilon\sigma_\ell (\varepsilon \geq 0.9)$ in the resonance region (data from ref. 1o).

Fig. 6: Comparison of the data on $\sigma_t + \varepsilon\sigma_\ell$ ($\varepsilon \geq 0.9$) at $q^2 = 0.1$ GeV^2 and $q^2 = 3$ GeV^2. The data at $q^2 = 0.1$ GeV^2 are renormalized to about 19 μb at W = 1.5 GeV.

Fig. 7a: $\sigma_t + \varepsilon\sigma_\ell (\varepsilon \geq 0.9)$ as function of q^2 at W = 1.275, 1.4, 1.5, 1.7 and 1.9 GeV as determined in ref. 1o.

b: Same as a) normalized to the ρ propagagor squared.

Fig. 8: Total cross section of the reaction $\gamma_v p \to \pi^- \Delta^{++}$ as measured by P. Joos et al.[19].

Fig. 9a: Nucleon axial vector form factor from pion electroproduction (refs. 15, 16, 17, 49). The curves show monopole and dipole fits to the $ep \to \pi^+ n$ data. The data on $ep \to \pi^- \Delta^{++}$ are not included into the fits.

b: q^2-dependence of the total cross section of $\gamma_v p \to \pi^- \Delta^{++}$

c: Nucleon axial vector form factor as determined from pion electroproduction (refs. 15, 16, 17) and $\pi^- \Delta^{++}$ production (ref. 18). The curves show dipole fits to the electroproduction data (solid line) and to the results of ν scattering (broken line) (from ref. 18).

Fig. 10: Example of a distribution of missing mass squared computed from the detected protons in coincidence with electrons, to identify π^o and η production (from ref. 38).

Fig. 11: Total cross section of $\gamma_v p \to \eta p$ at W = 1.535 GeV as function of q^2. In comparison the total cross section of $\gamma_v p \to X$ renormalized to 12.5 μb at $q^2 = 0$.

Fig. 12: Preliminary distribution of missing mass squared computed from detected protons in coincidence with electrons at $\varepsilon \approx 0.5$, $1.49 < W < 1.58$ GeV, $q^2 = 1$ GeV^2.

Fig. 13: Forward π^+ production at $q^2 = 0.4$ GeV^2 from DNPL[36] and at $q^2 = 0.6$ and 1 GeV^2 from DESY[37]. Solid line: fit 1, broken line: fit 2 (see text, 5.4).

Fig. 14: Backward π^o production at $q^2 \approx 0.6$ GeV^2 from DNPL and at $q^2 \approx 0.6$ and 1 GeV^2 from DESY. Solid line: fit 1, broken line: fit 2 (see text, 5.4).

Fig. 15: W-dependence of $\gamma_v p \to \pi^+ n$ at $\Theta^*_{\pi^+} = 90^o$, 80^o, 70^o and 60^o at $q^2 = 1.2$ GeV^2 (from ref. 4o).

Fig. 16: Examples of angular distributions of $\gamma_v p \to \pi^o p$ at $q^2 \approx 0.6$ GeV^2 from DESY[38] in comparison with data from DNPL[39]. Curves: cross section computed from the angular coefficients as fitted to the DESY data (see text).

Fig. 17: Examples of angular distributions of $\gamma_v p \to \pi^o p$ at $q^2 \approx 1$ GeV^2 (data from ref. 38,42). Curves: fit 1 (see text, 5.4).

Fig. 18: $\gamma_v p \to \pi^o p$. Angular distributions of $\sigma_U + \varepsilon\sigma_L$ (△), σ_P (□) and σ_I (O) at $q^2 \approx 1$ GeV^2 (data from ref. 38). Curves: $\sigma_U + \varepsilon\sigma_L$ (———), σ_P (--) and σ_I (....) as computed from fit 1 (see text, 5.4).

Fig. 19: Angular coefficients $\overline{A}_o$, $\overline{A}_2$ and C_o at $q^2 \approx 1$ GeV^2. Data below W = 1.325 GeV from ref. 26, above from ref. 42.

Fig. 2o: Total cross section of $\gamma_v p \to \pi^o p$ (▽ from ref. 43, ✳ from ref. 39, ▼ from ref. 38) in comparison to the total cross section of $\gamma_v p \to X$ (O from ref. 1o).

Fig. 21: Examples of angular distributions of $\gamma_v p \to \pi^+ n$ at $q^2 \approx 1$ GeV^2 (data from ref. 37). Solid line: fit 1 (see text, 5.4).

Fig. 22: Same as fig. 18 in the case of $\gamma_v p \to \pi^+ n$.

Fig. 23: Solutions of Devenish and Lyth[3] evaluated at the resonance position together with the results of fit 1 (▽) and fit 2 (△) (see text, 5.4). The couplings are given for the channel $ep \to ep\pi^o$ in $(\mu b)^{1/2}$.

Fig. 24: Solutions of Devenish and Lyth[3] for the helicity ratios of $D_{13}(152o)$ and $F_{15}(1688)$ together with the results of fit 1 (▽) and fit 2 (△) (see text, 5.4).

Fig. 25: Results of fit 1 (▼) and fit 2 (▲) (see text) on the helicity asymmetries of $D_{13}(152o)$ and $F_{15}(1688)$ off protons, together with the results of Devenish and Lyth[3] (DL), and the predictions of Ravndal[46] (R), Ono[47] (O) and Körner et al.[48] (KBA).

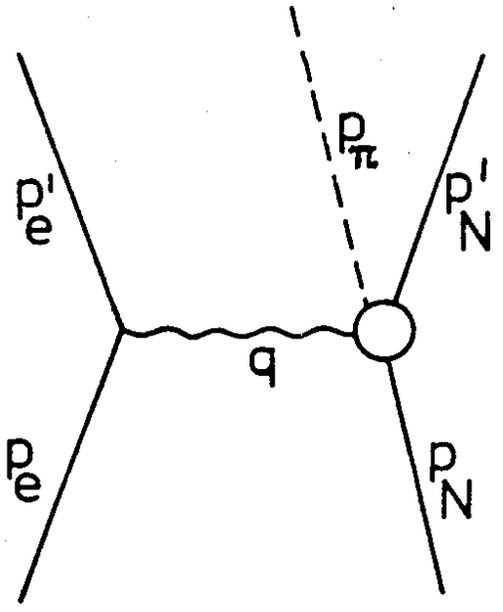
p_π
p'_e
p'_N
q
p_e
p_N

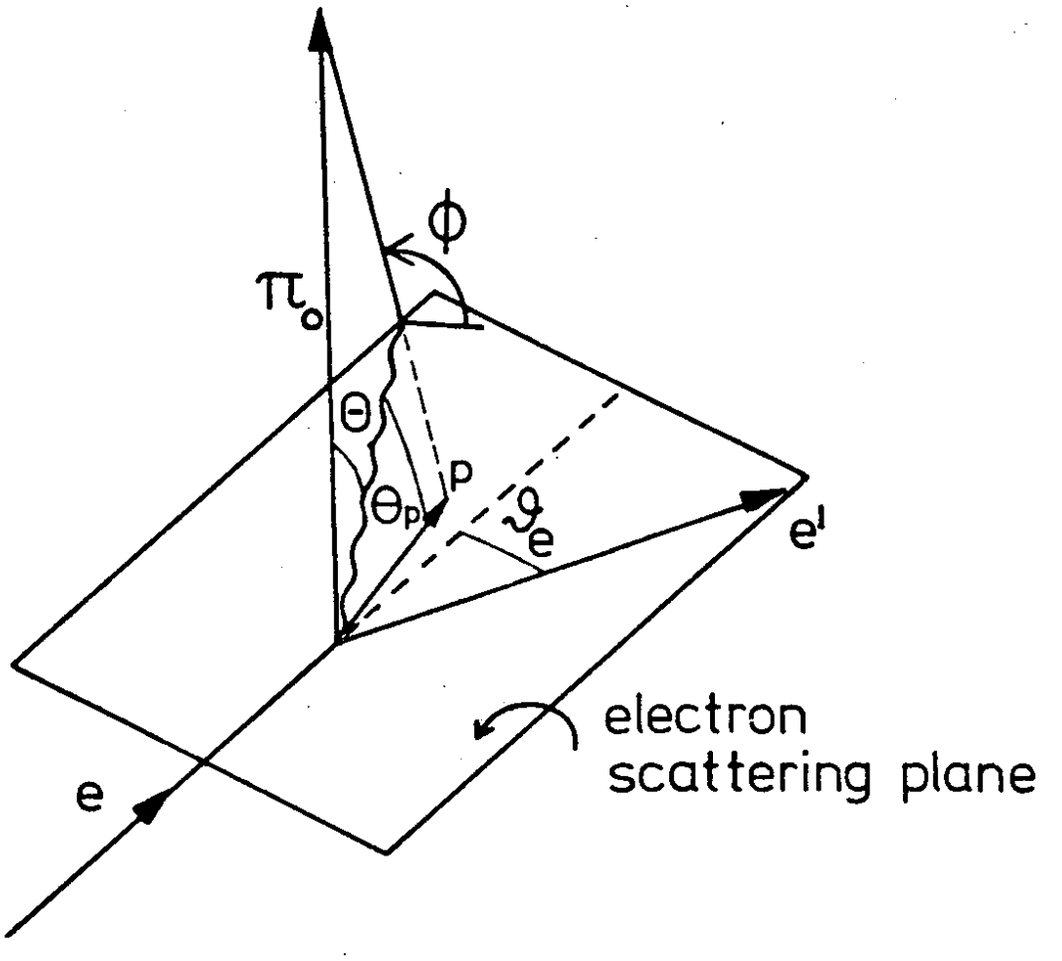
ϕ
π_o
Θ
Θ_p
p
ϑ_e
e'
electron
scattering plane
e

Fig. 1

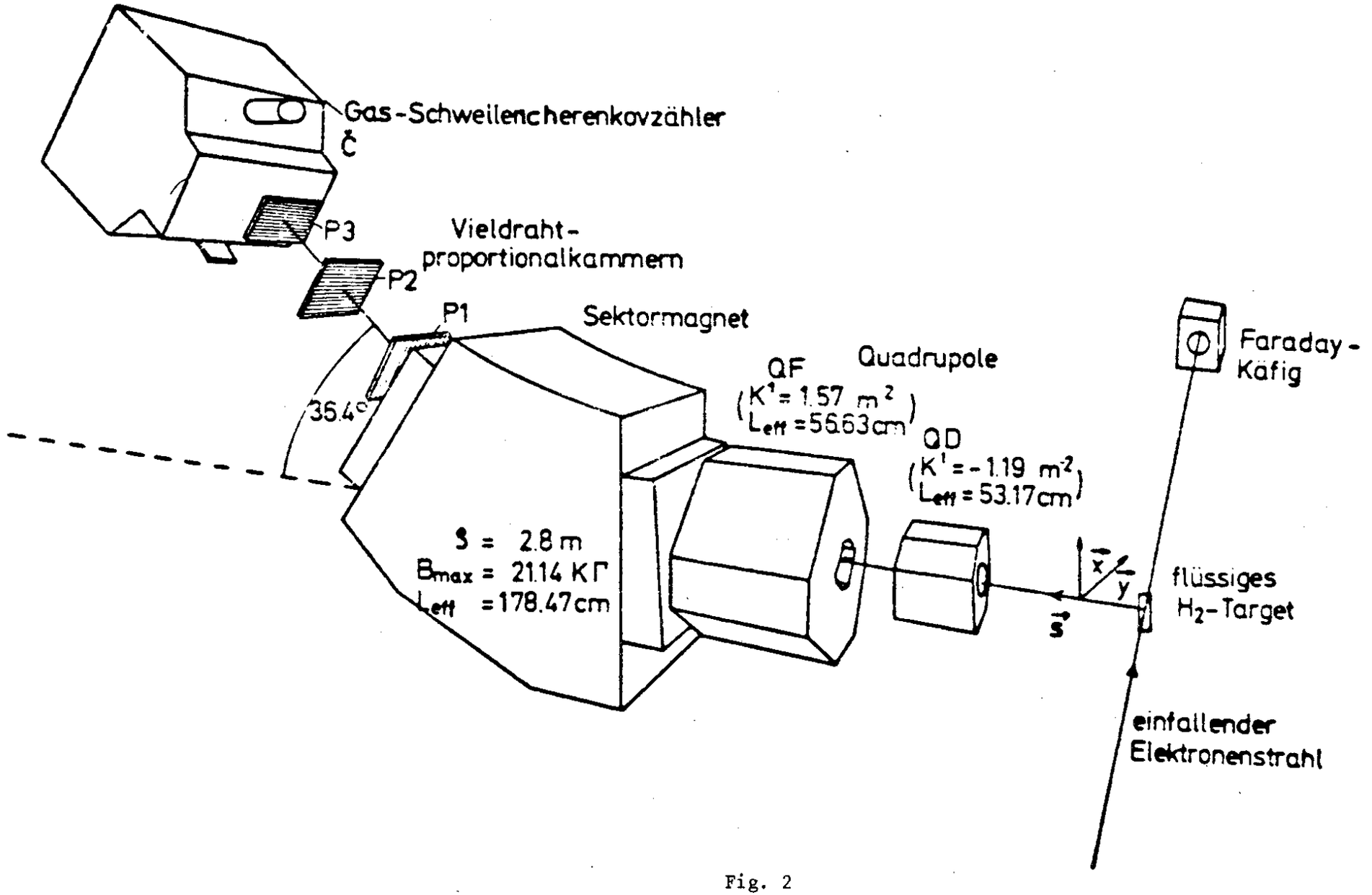
Gas-Schwellencherenkovzähler
Č
P3
Vieldraht-
proportionalkammern
P2
P1
Sektormagnet
36.4°
QF
Quadrupole
(K¹ = 1.57 m²
Leff = 56.63cm)
QD
(K¹ = -1.19 m²
Leff = 53.17cm)
S = 2.8 m
Bmax = 21.14 KΓ
Leff = 178.47cm
Faraday-
Käfig
flüssiges
H2-Target
einfallender
Elektronenstrahl

Fig. 2

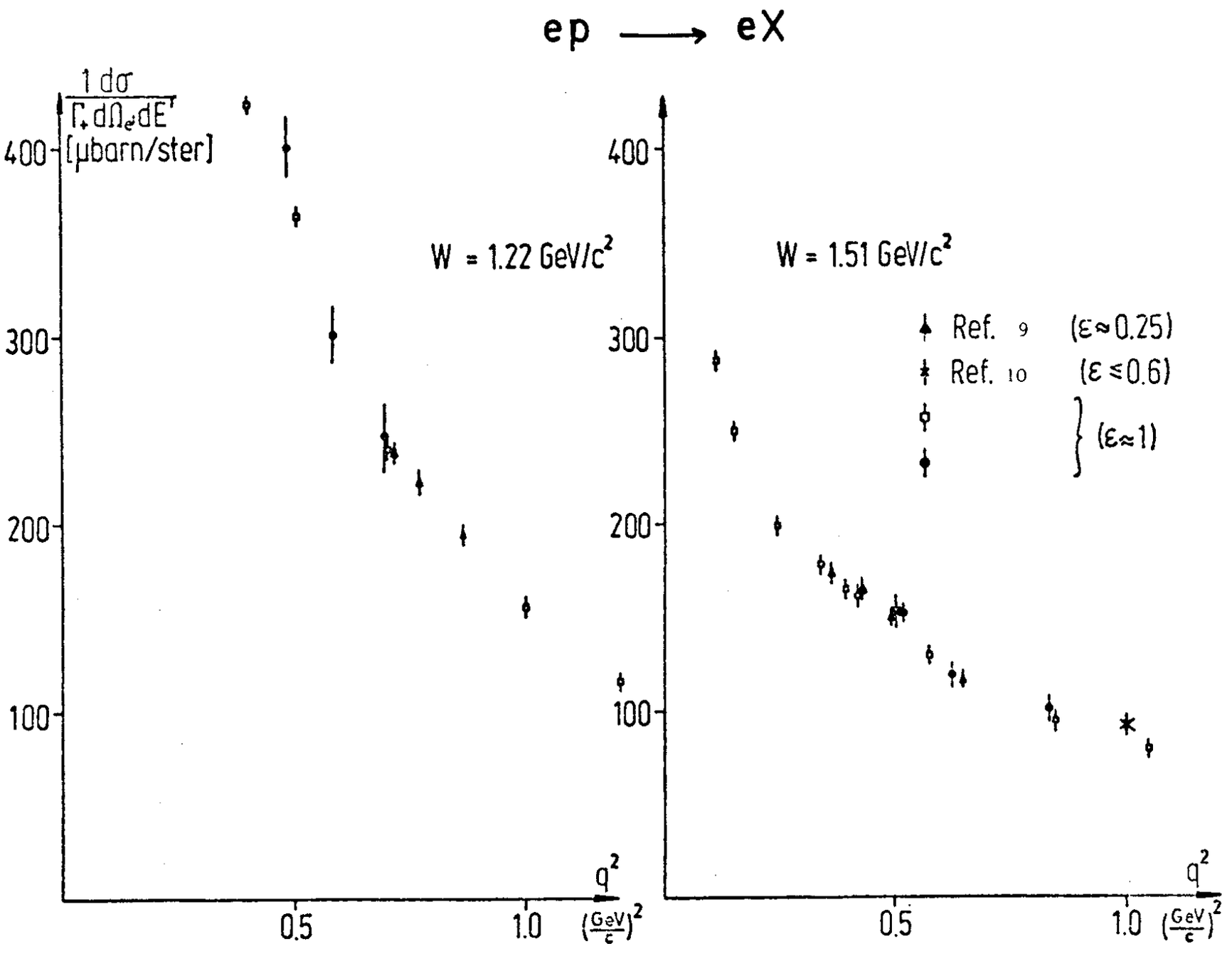
ep ⟶ eX
1 dσ / Γ_v dΩ_e dE'
[μbarn/ster]
400
300
200
100
W = 1.22 GeV/c²
W = 1.51 GeV/c²
Ref. 9 (ε≈0.25)
Ref. 10 (ε≤0.6)
(ε≈1)
q²
0.5
1.0
(GeV/c)²

Fig. 3

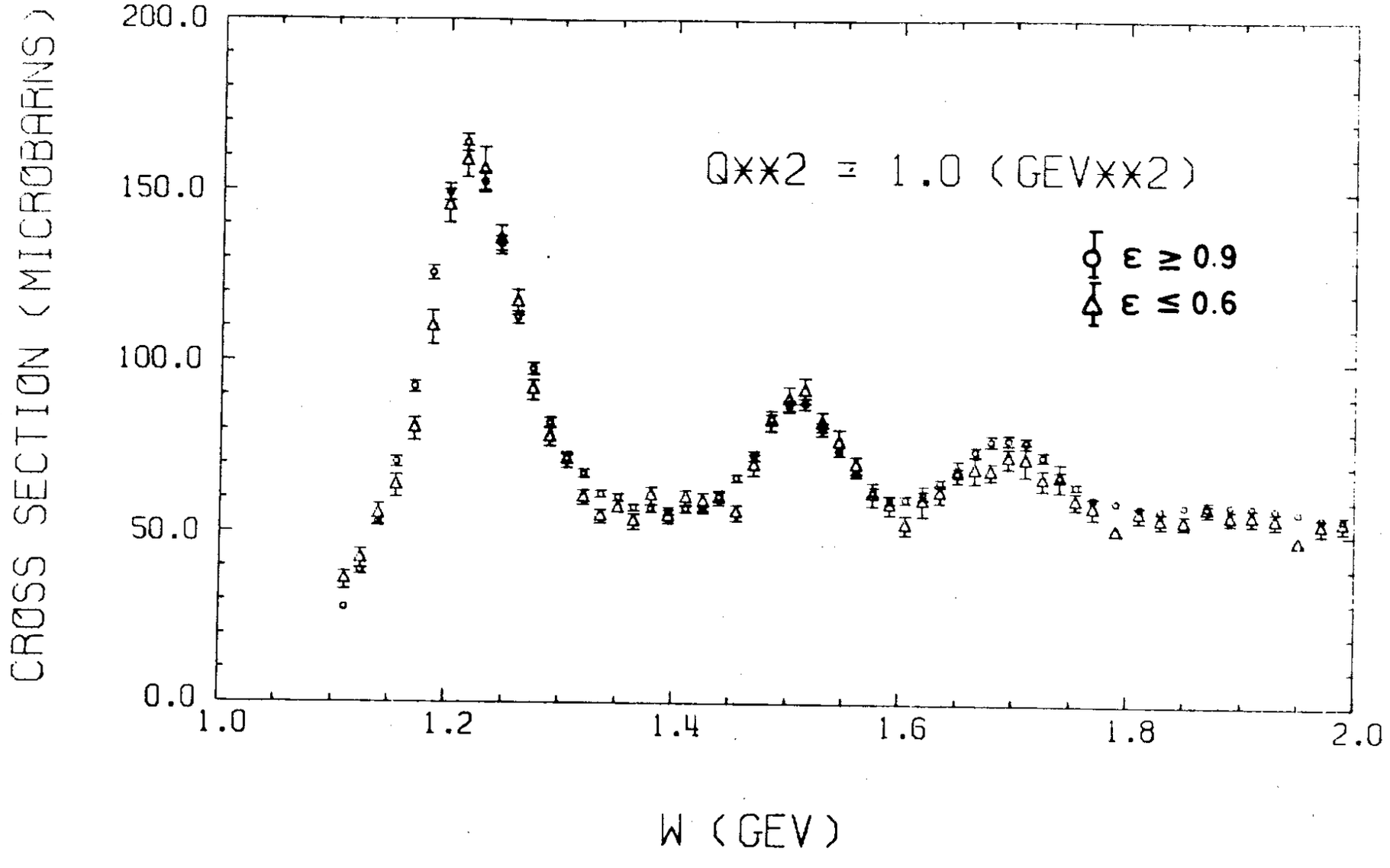
CROSS SECTION (MICROBARNS)
200.0
150.0
100.0
50.0
0.0
1.0
1.2
1.4
1.6
1.8
2.0
W (GEV)
Q**2 = 1.0 (GEV**2)
ε ≥ 0.9
ε ≤ 0.6

Fig. 4

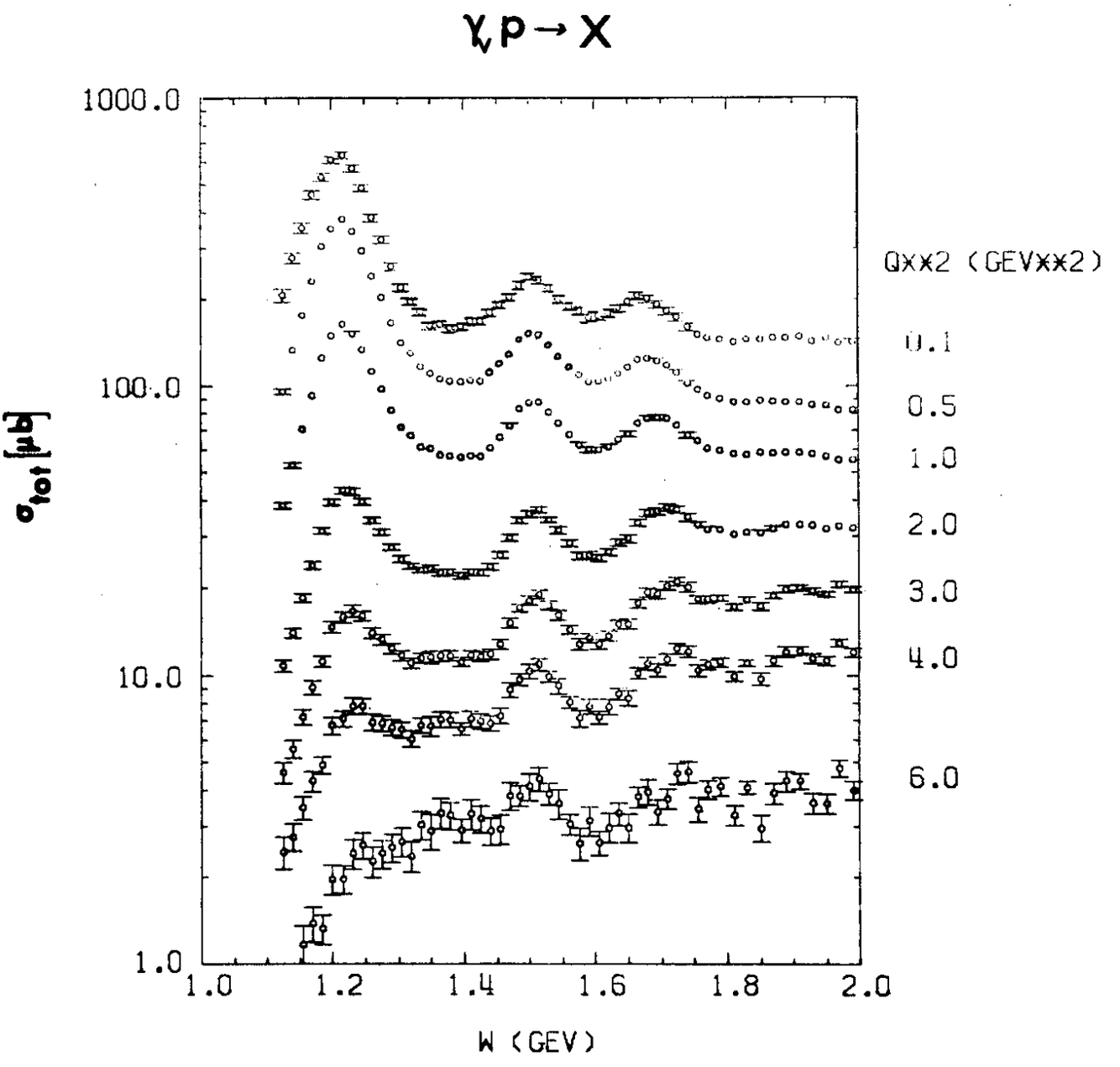
γ_v p → X
1000.0
100.0
10.0
1.0
σ_tot [μb]
1.0
1.2
1.4
1.6
1.8
2.0
W (GEV)
Q**2 (GEV**2)
0.1
0.5
1.0
2.0
3.0
4.0
6.0

Fig. 5

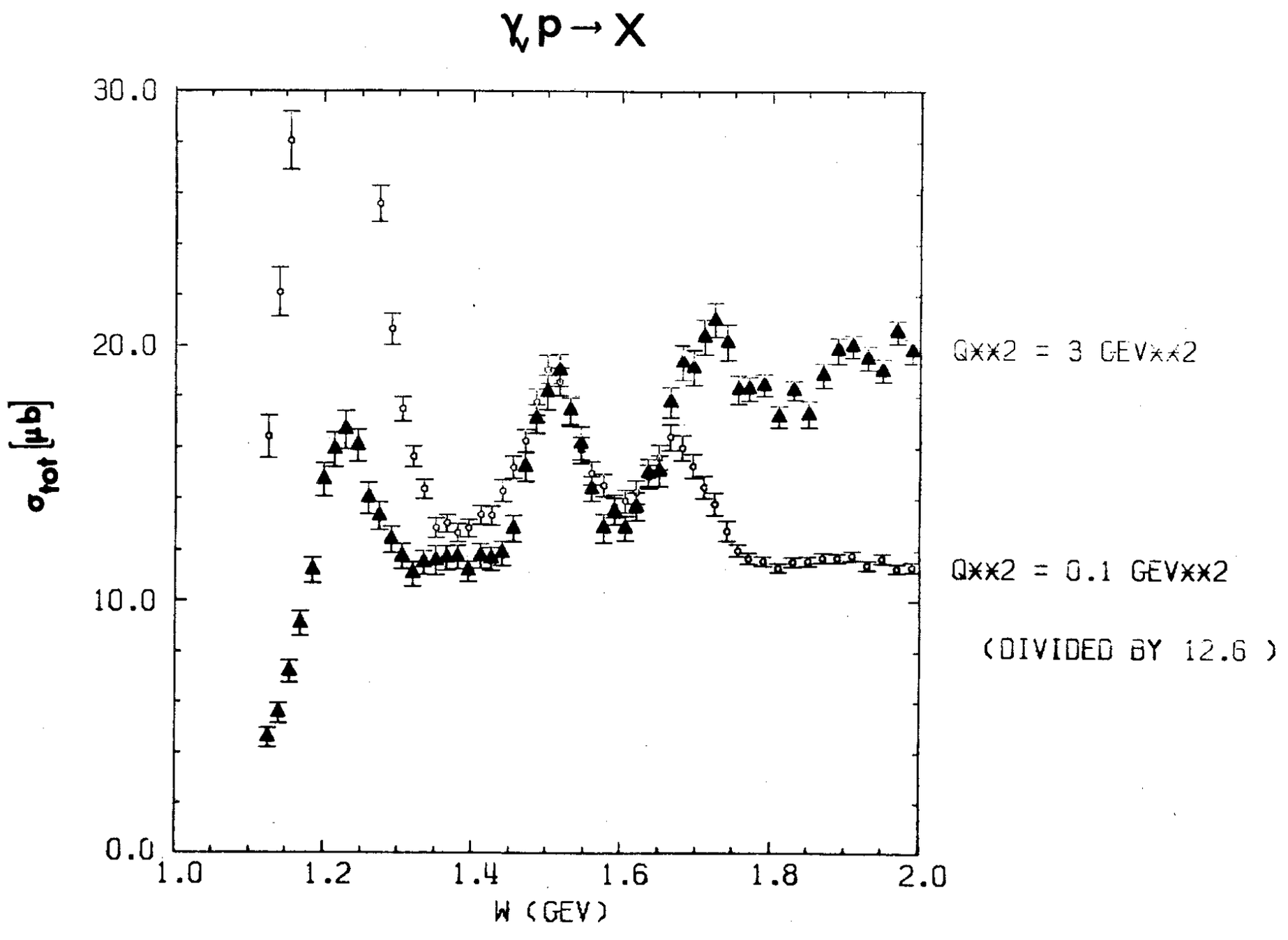
γ,p → X
30.0
20.0
10.0
0.0
1.0
1.2
1.4
1.6
1.8
2.0
W (GEV)
σtot [μb]
Q**2 = 3 GEV**2
Q**2 = 0.1 GEV**2
(DIVIDED BY 12.6)

Fig. 6

$\gamma, p \to X$

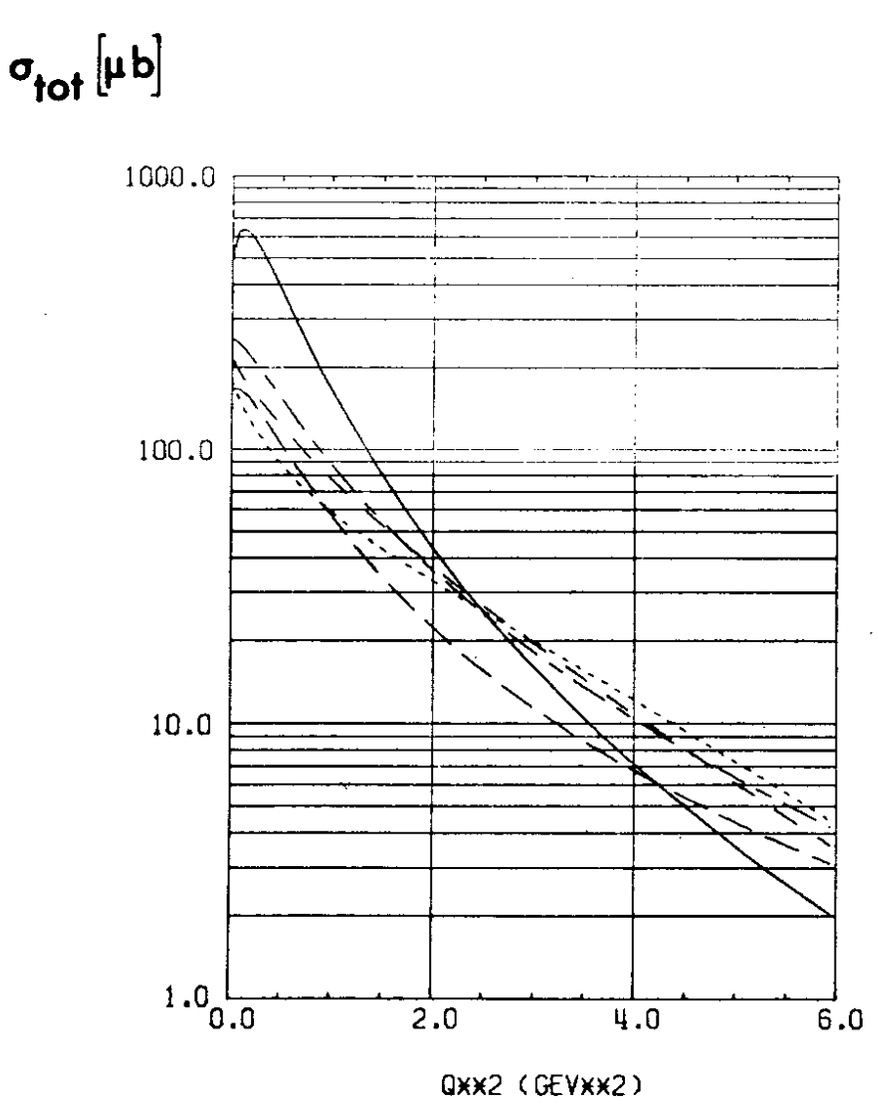

Fig. 7a

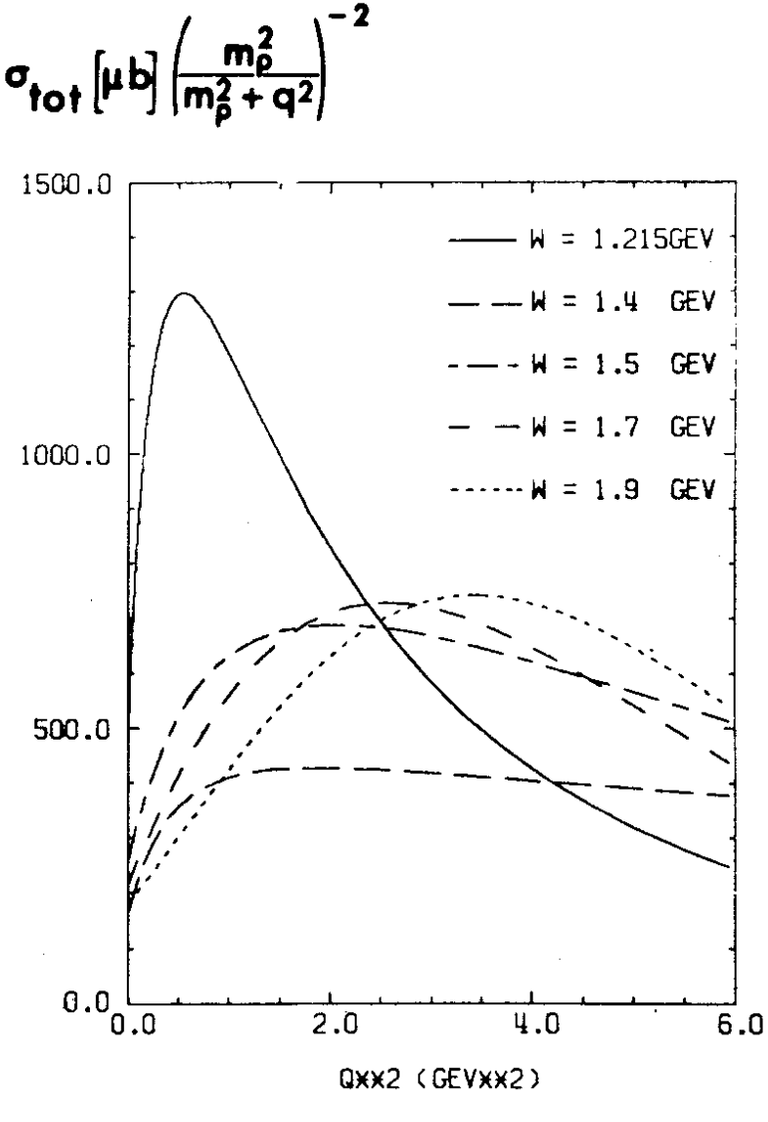

Fig. 7b

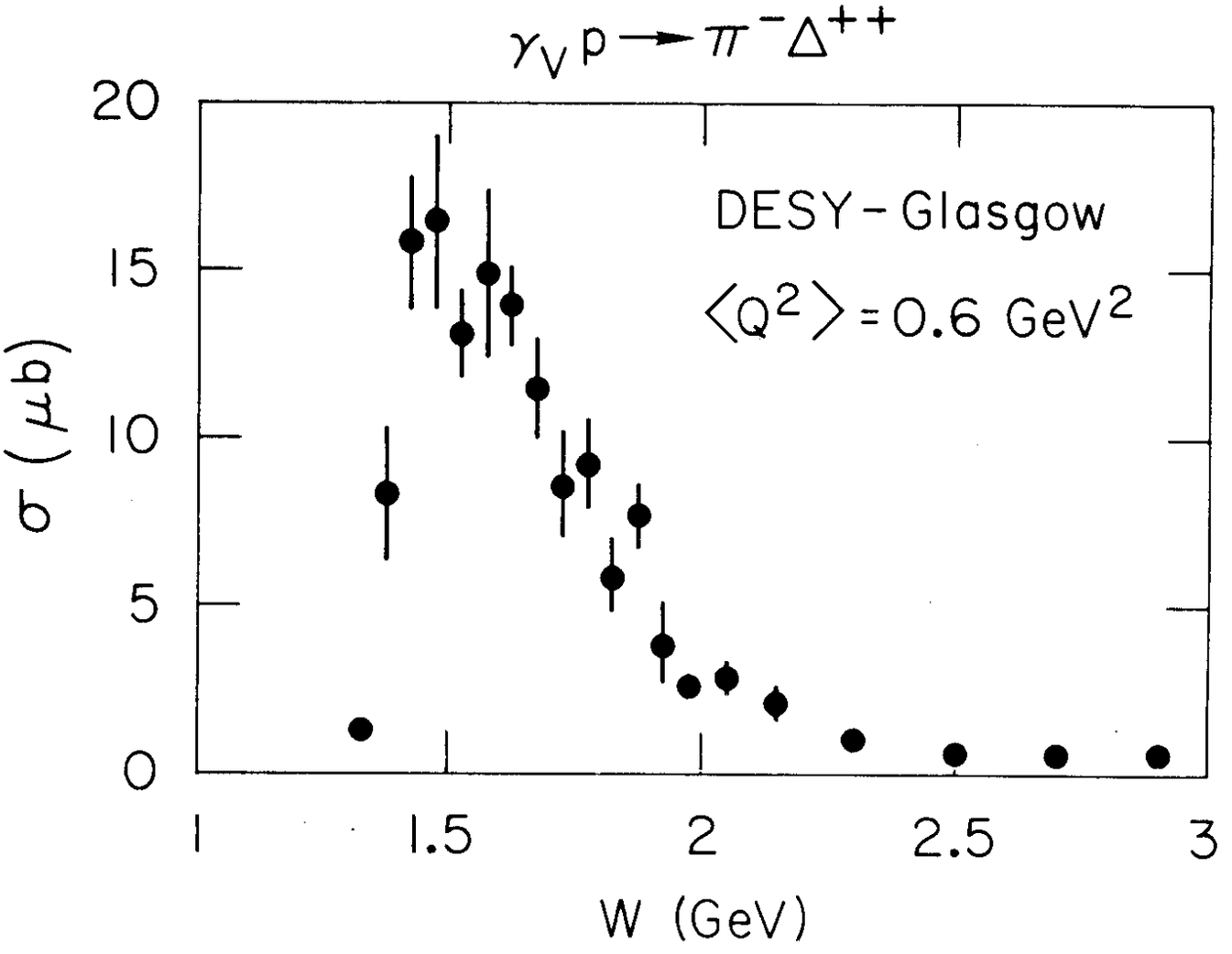
$\gamma_V p \rightarrow \pi^- \Delta^{++}$
DESY - Glasgow
$\langle Q^2 \rangle = 0.6$ GeV^2
σ (μb)
W (GeV)
0
5
10
15
20
1
1.5
2
2.5
3

Fig. 8

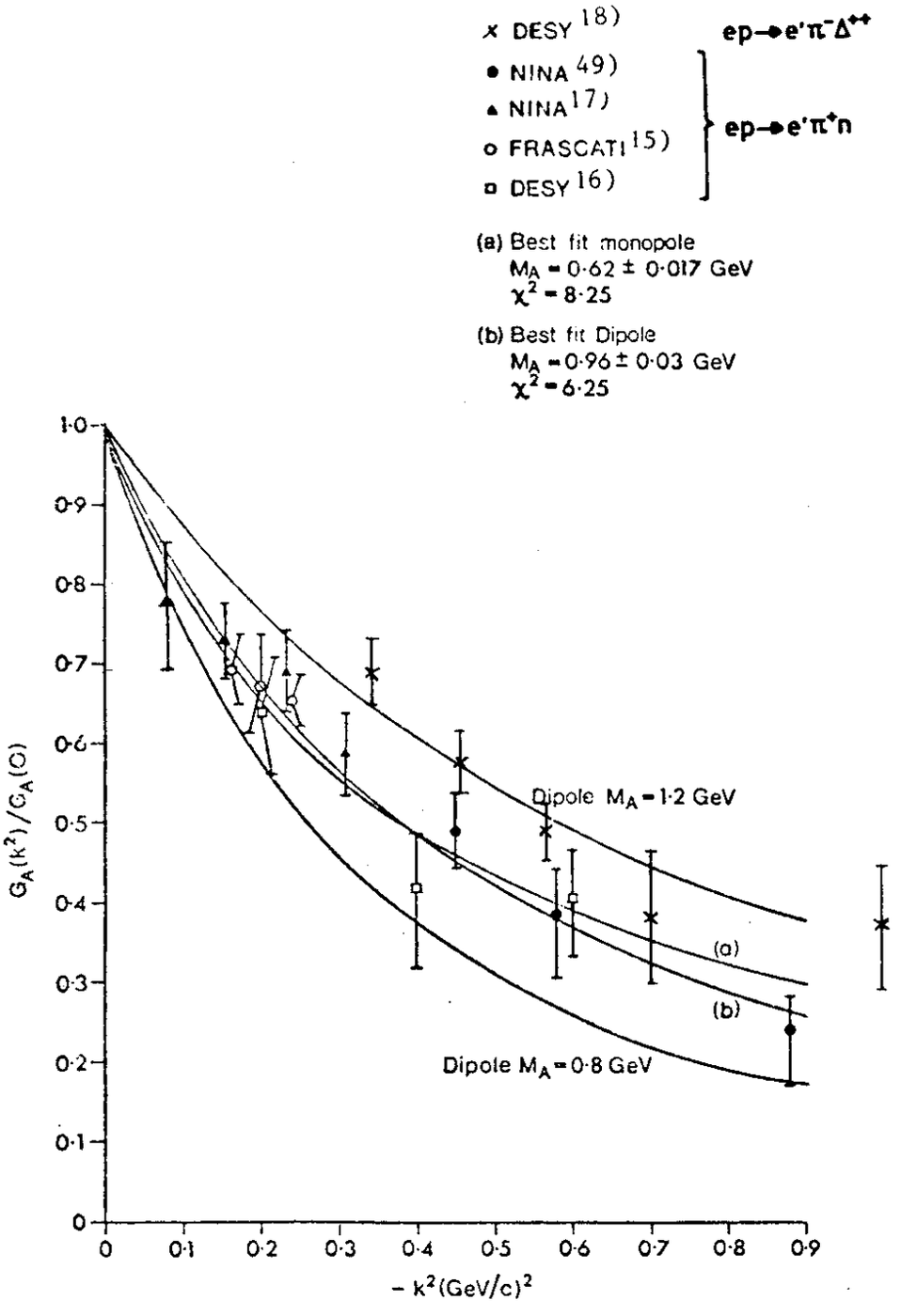
× DESY [18]
ep→e'π⁻Δ⁺⁺
● NINA [49]
▲ NINA [17]
○ FRASCATI [15]
□ DESY [16]
ep→e'π⁺n
(a) Best fit monopole
M_A = 0·62 ± 0·017 GeV
χ^2 = 8·25
(b) Best fit Dipole
M_A = 0·96 ± 0·03 GeV
χ^2 = 6·25
Dipole M_A = 1·2 GeV
(a)
(b)
Dipole M_A = 0·8 GeV
$G_A(k^2)/G_A(0)$
$-k^2$(GeV/c)²
1·0
0·9
0·8
0·7
0·6
0·5
0·4
0·3
0·2
0·1
0
0·1
0·2
0·3
0·4
0·5
0·6
0·7
0·8
0·9

Fig. 9a

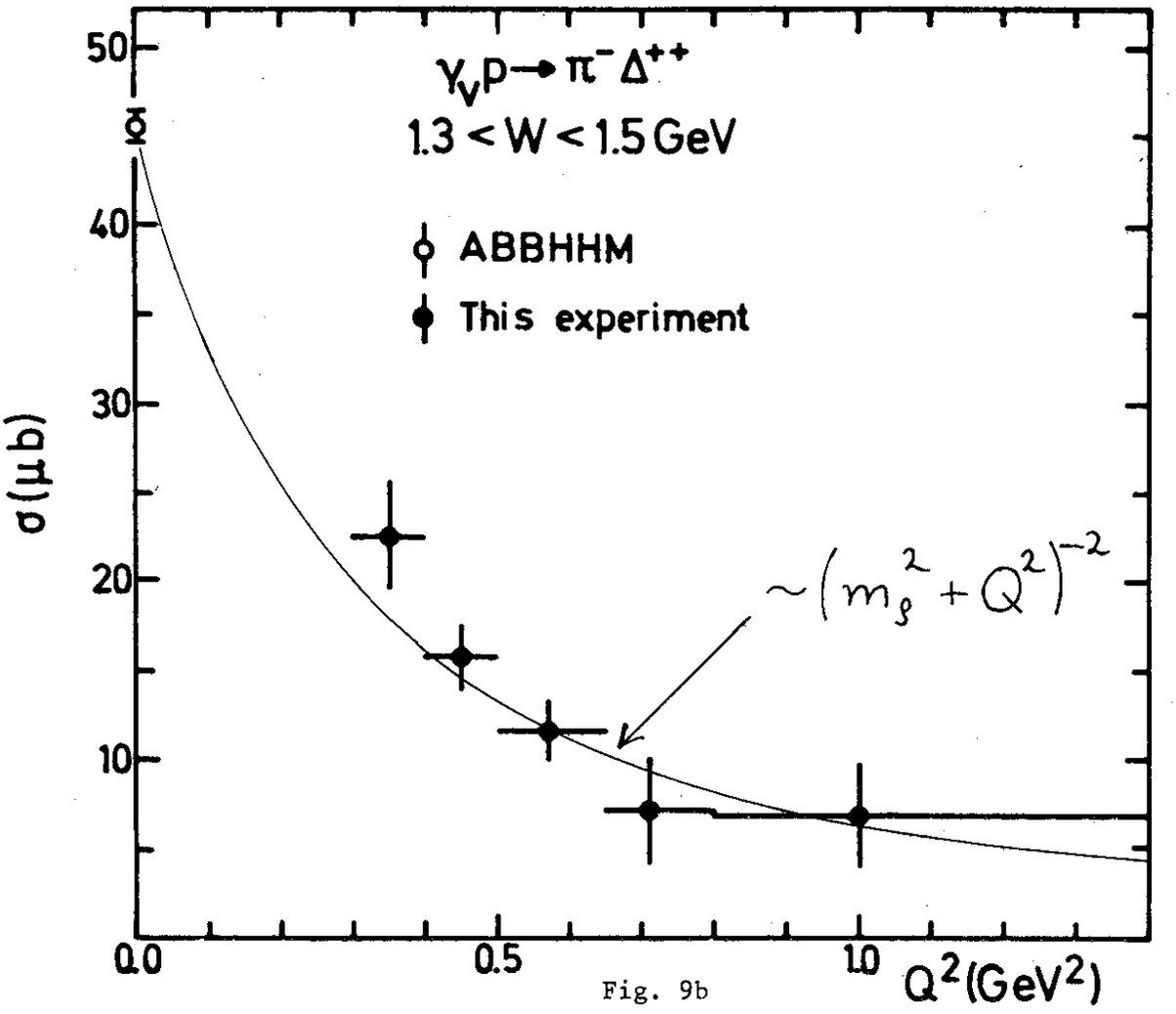
$\gamma_V p \to \pi^- \Delta^{++}$
$1.3 < W < 1.5\,GeV$
ABBHHM
This experiment
$\sim (m_\rho^2 + Q^2)^{-2}$
$\sigma(\mu b)$
$Q^2(GeV^2)$
0.0
0.5
1.0
10
20
30
40
50

Fig. 9b

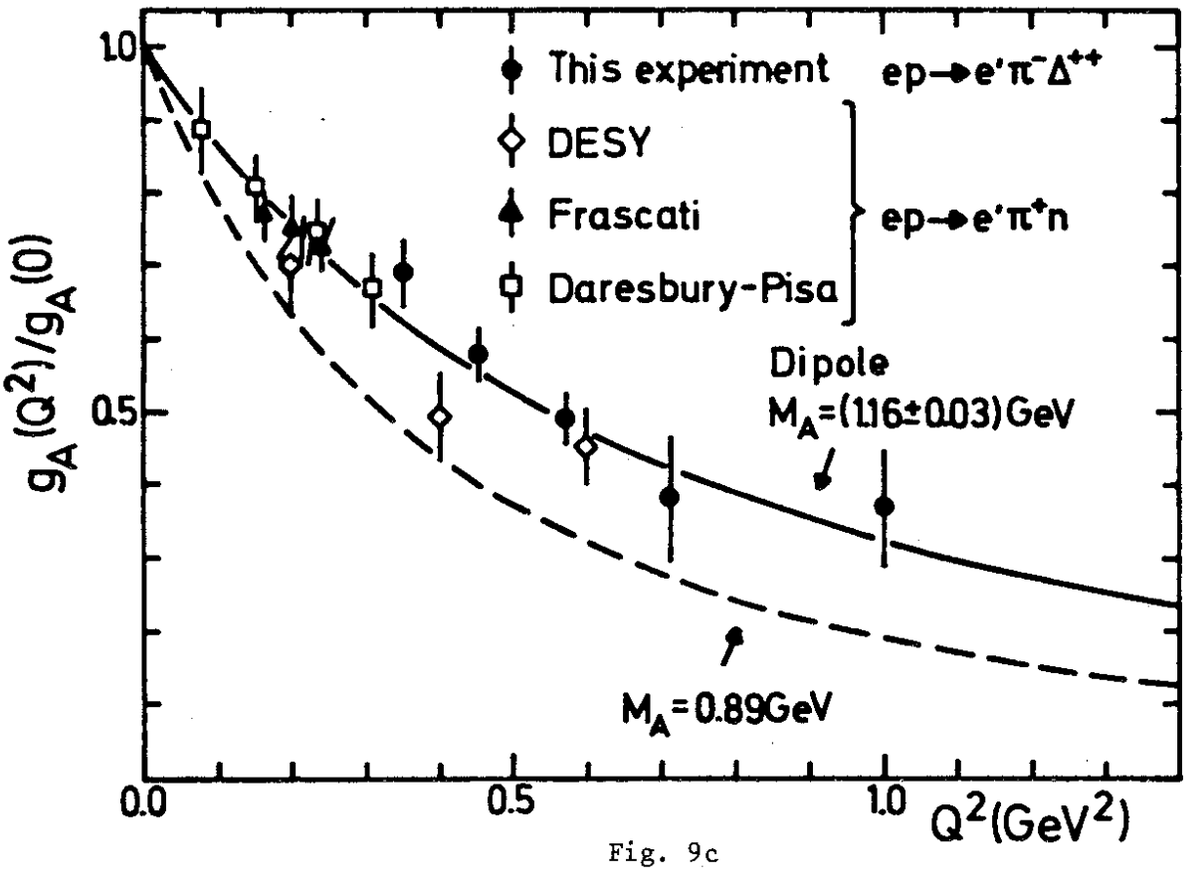
This experiment
$ep \to e'\pi^-\Delta^{++}$
DESY
Frascati
Daresbury-Pisa
$ep \to e'\pi^+ n$
Dipole
$M_A = (1.16 \pm 0.03)\,GeV$
$M_A = 0.89\,GeV$
$g_A(Q^2)/g_A(0)$
$Q^2(GeV^2)$
0.0
0.5
1.0

Fig. 9c

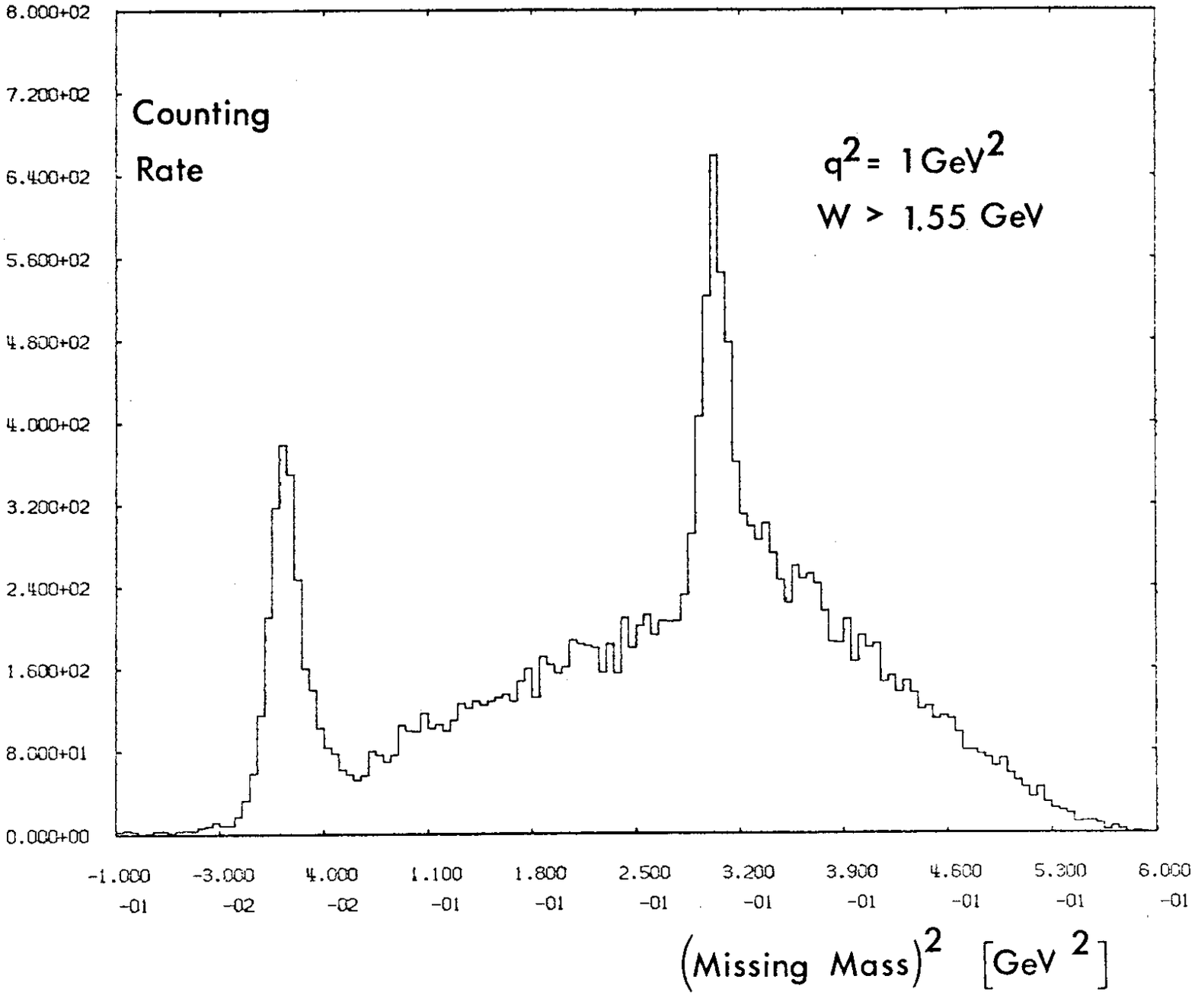
Counting
Rate
$q^2 = 1 GeV^2$
W > 1.55 GeV
8.000+02
7.200+02
6.400+02
5.600+02
4.800+02
4.000+02
3.200+02
2.400+02
1.600+02
8.000+01
0.000+00
-1.000 -01
-3.000 -02
4.000 -02
1.100 -01
1.800 -01
2.500 -01
3.200 -01
3.900 -01
4.600 -01
5.300 -01
6.000 -01
$(Missing\ Mass)^2$ $[GeV^2]$

Fig. 10

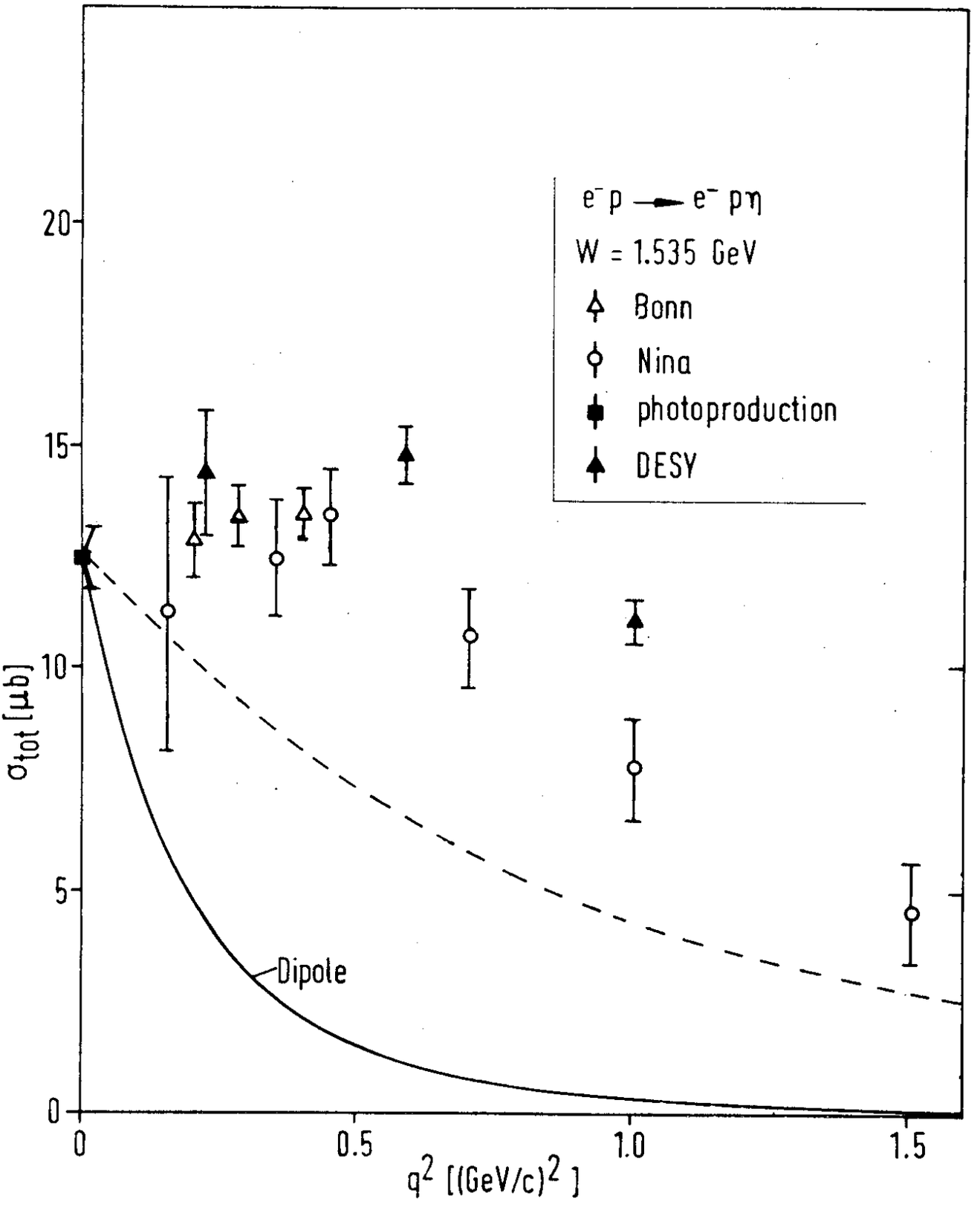
e⁻ p → e⁻ pη
W = 1.535 GeV
Bonn
Nina
photoproduction
DESY
Dipole
σtot [μb]
q² [(GeV/c)²]
0
5
10
15
20
0
0.5
1.0
1.5

Fig. 11

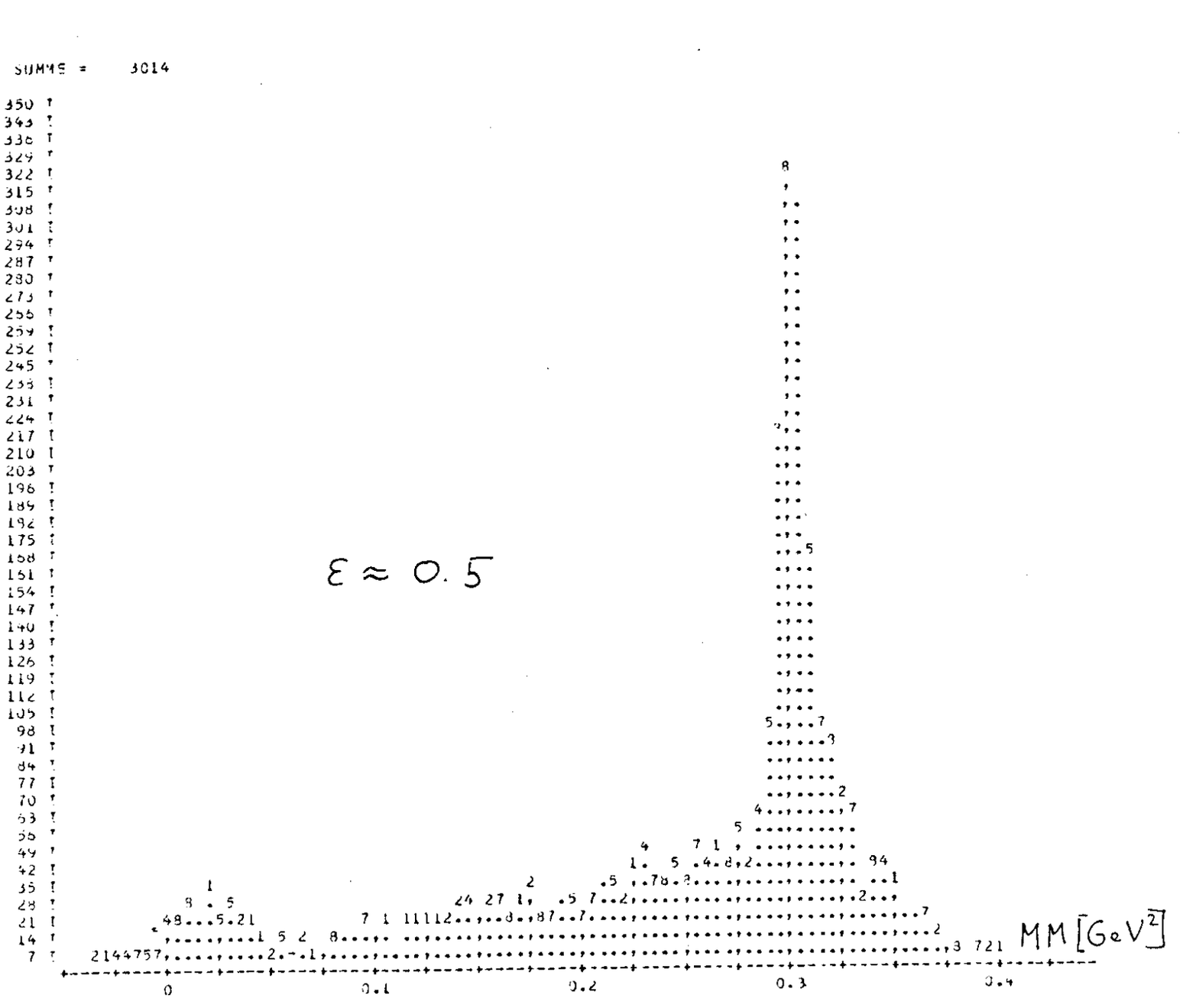

Fig. 12

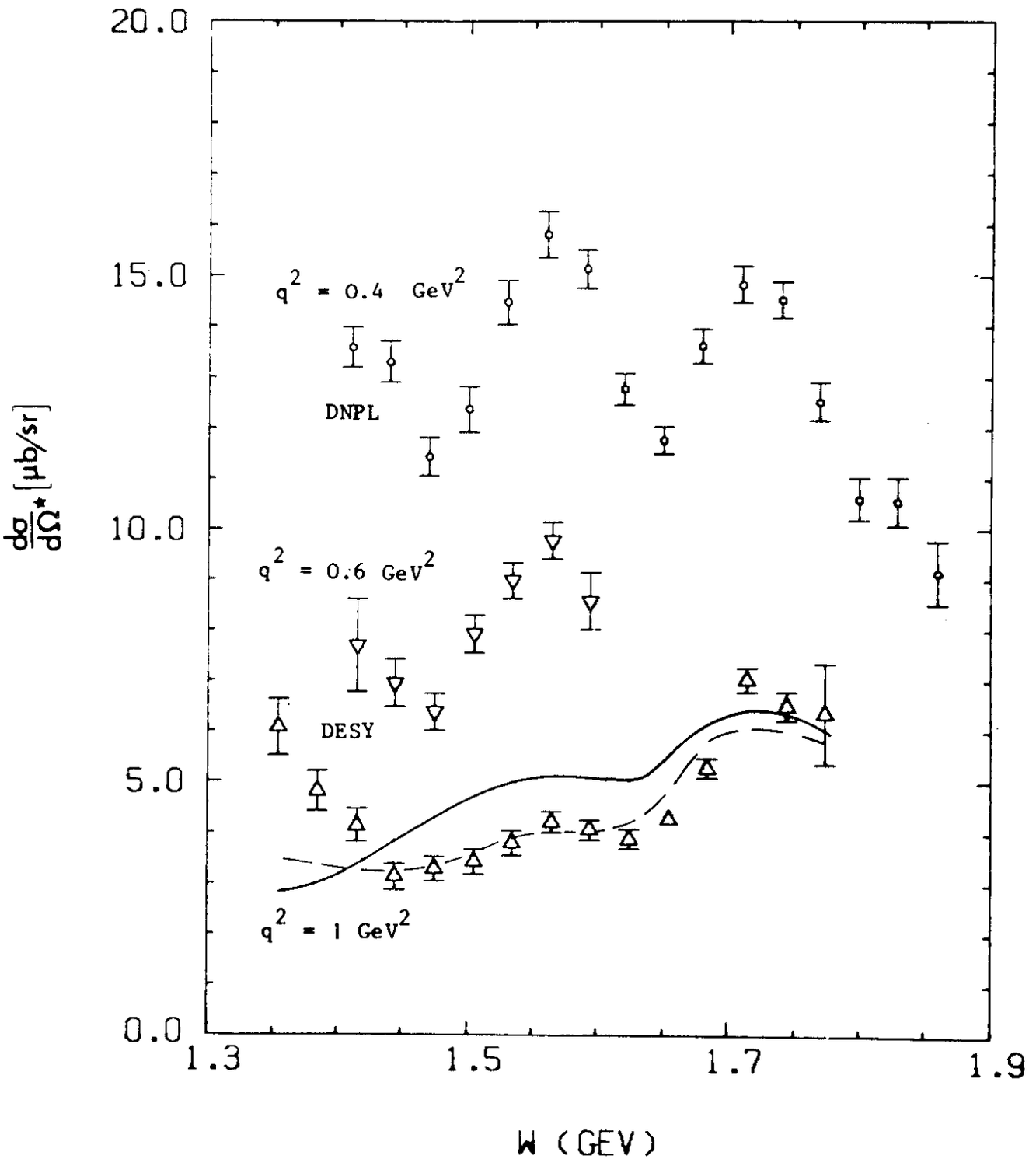
$\gamma_v p \rightarrow \pi^+ n$
$\theta^*_{\pi^+} \approx 0°$
20.0
15.0
10.0
5.0
0.0
1.3
1.5
1.7
1.9
W (GEV)
$\frac{d\sigma}{d\Omega^*}$ [μb/sr]
q^2 = 0.4 GeV^2
DNPL
q^2 = 0.6 GeV^2
DESY
q^2 = 1 GeV^2

Fig. 13

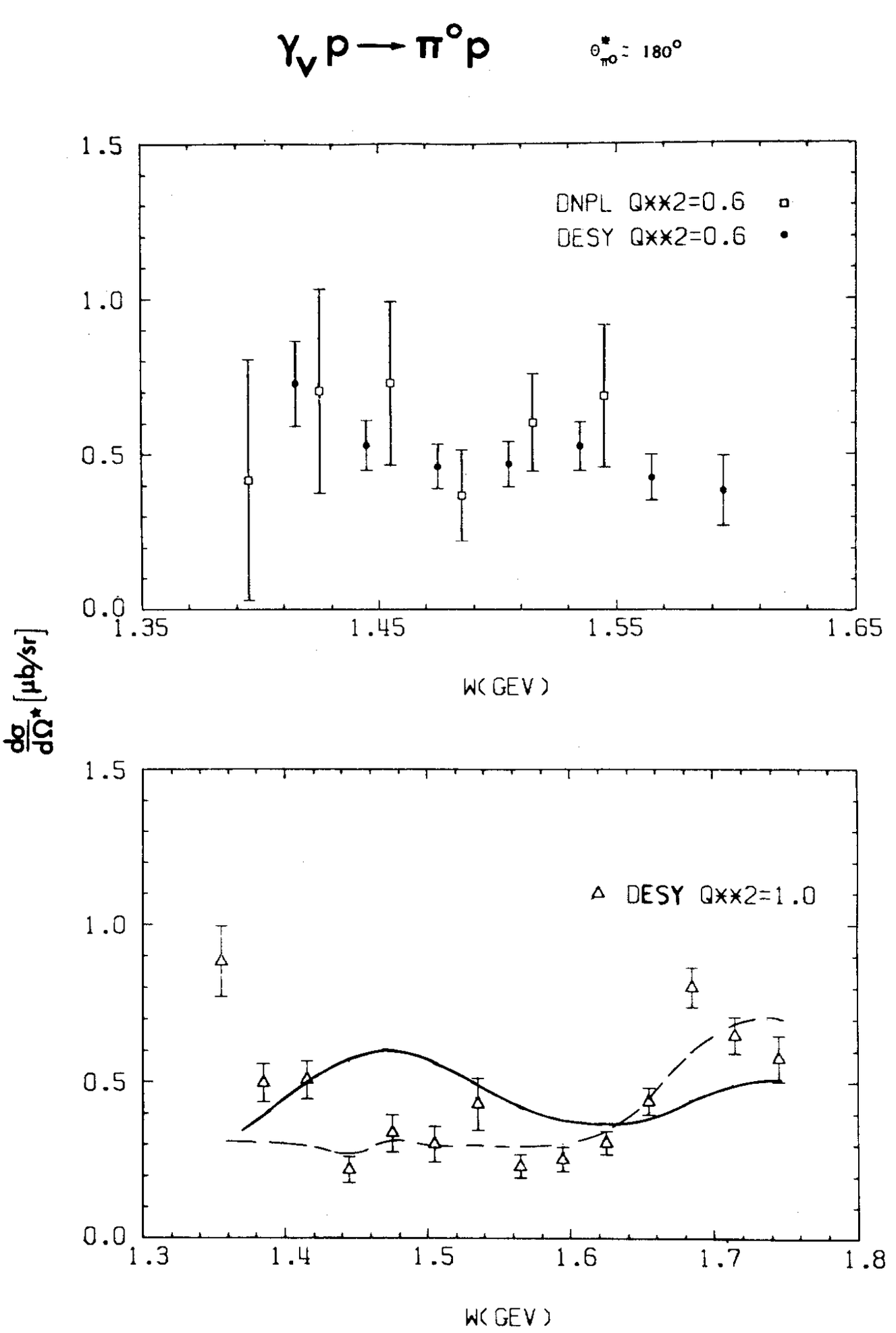
$\gamma_v p \rightarrow \pi^0 p$
$\theta^*_{\pi^0} = 180°$
DNPL Q**2=0.6
DESY Q**2=0.6
DESY Q**2=1.0
$\frac{d\sigma}{d\Omega^*}$ [μb/sr]
W(GEV)
W(GEV)

Fig. 14

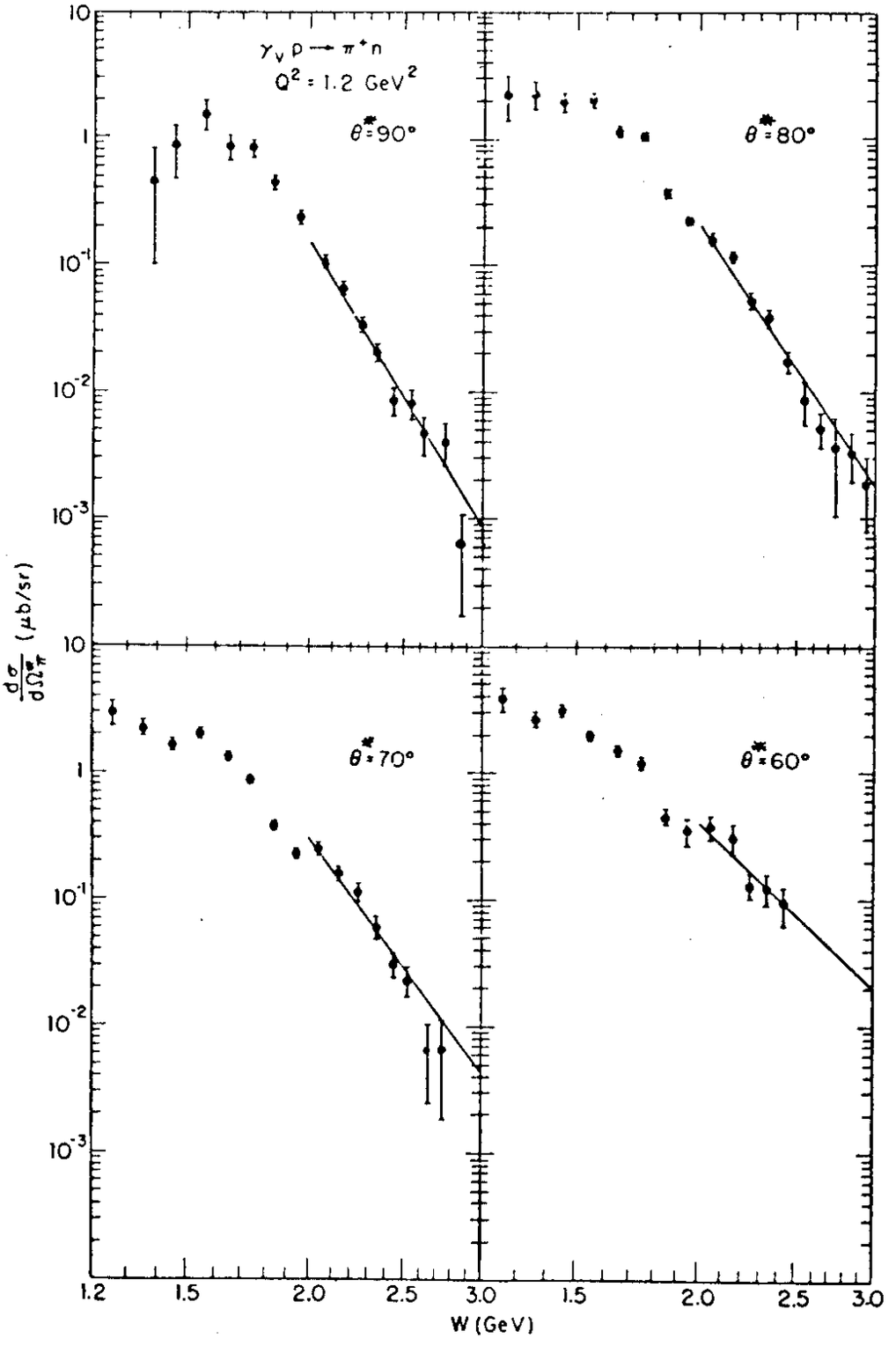
$\gamma_v p \rightarrow \pi^+ n$
$Q^2 = 1.2$ GeV^2
$\theta^* = 90°$
$\theta^* = 80°$
$\theta^* = 70°$
$\theta^* = 60°$
$\frac{d\sigma}{d\Omega_\pi^*}$ (μb/sr)
W (GeV)
10
1
10^{-1}
10^{-2}
10^{-3}
1.2
1.5
2.0
2.5
3.0

Fig. 15

$\gamma_v p \rightarrow \pi^0 p$

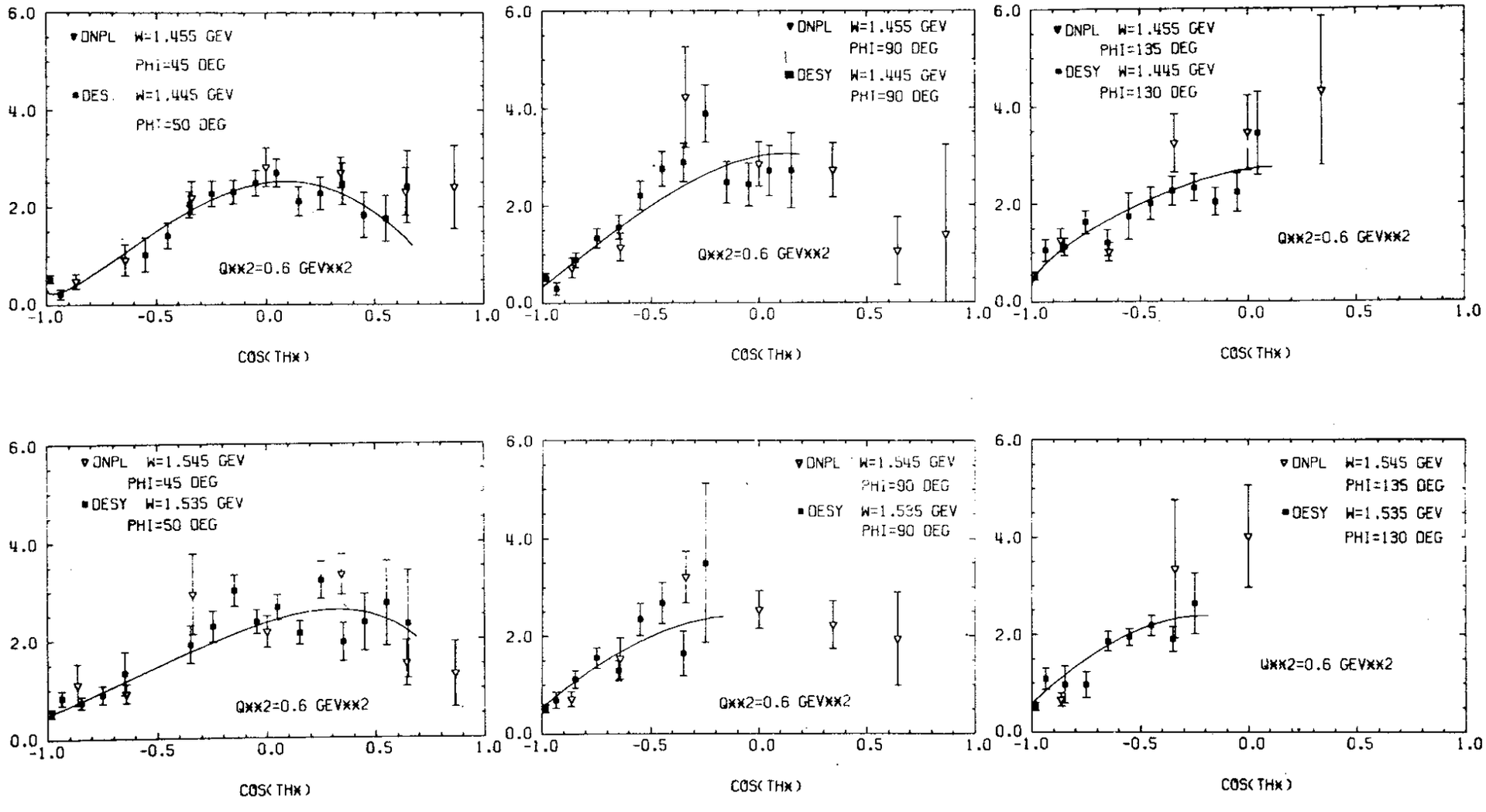

Fig. 16

$\gamma_v p \rightarrow \pi^0 p$

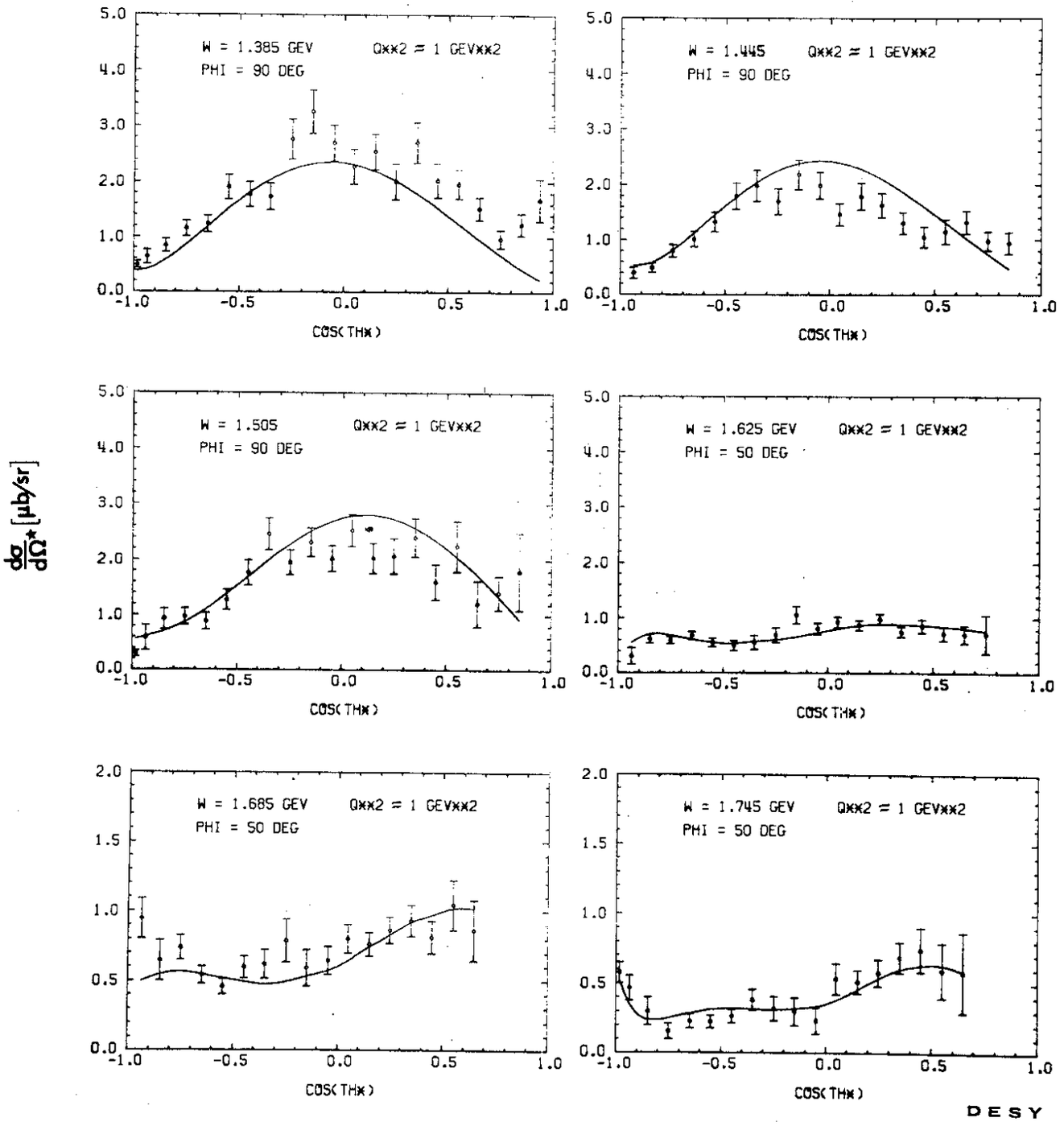

Fig. 17

$\gamma_v p \rightarrow \pi^0 p$

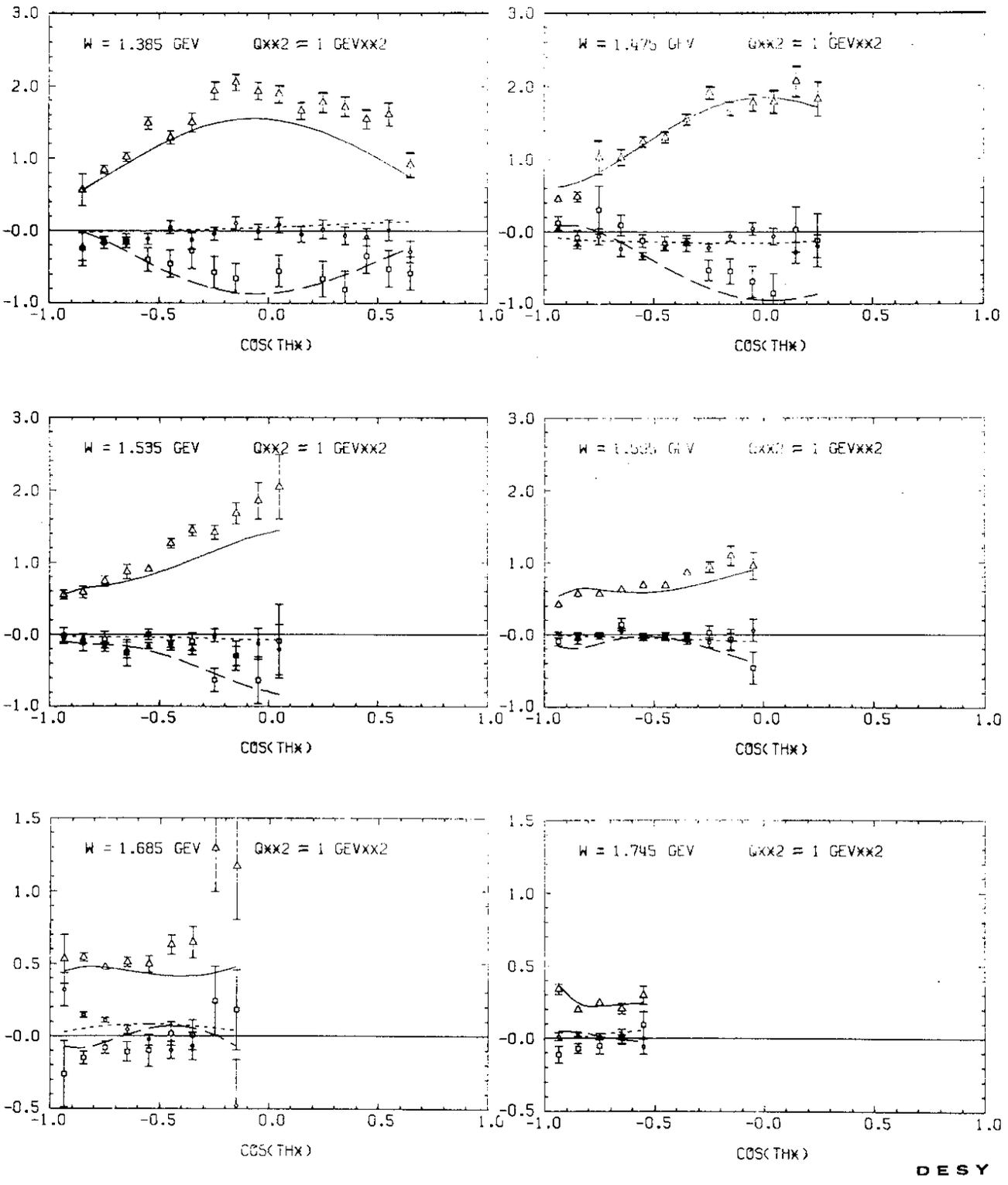

Fig. 18

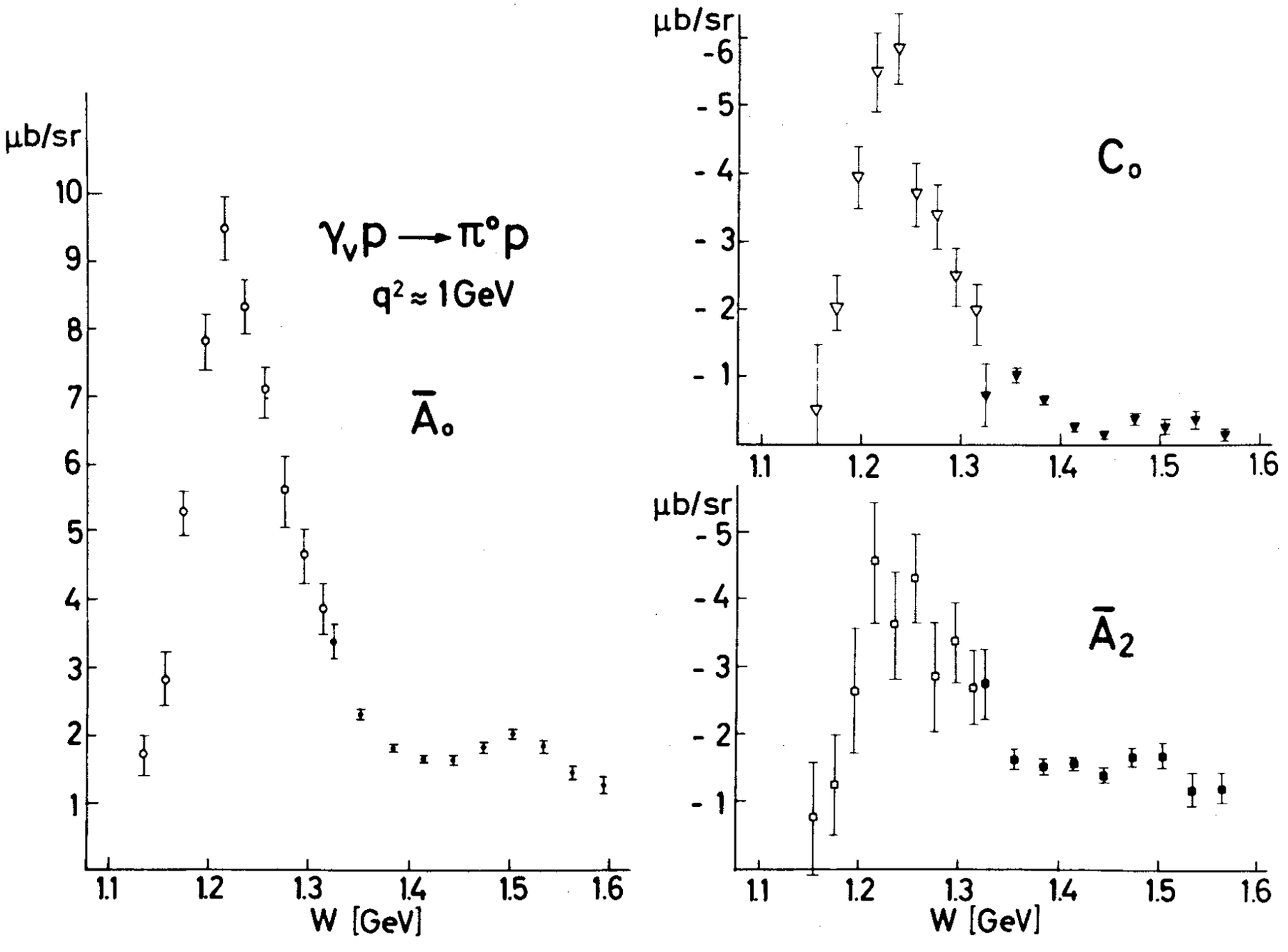
μb/sr
10
9
8
7
6
5
4
3
2
1
$\gamma_v p \longrightarrow \pi^\circ p$
$q^2 \approx 1\,GeV$
$\bar{A}_o$
1.1
1.2
1.3
1.4
1.5
1.6
W [GeV]
μb/sr
-6
- 5
- 4
- 3
- 2
- 1
C_o
1.1
1.2
1.3
1.4
1.5
1.6
μb/sr
- 5
- 4
- 3
- 2
- 1
$\bar{A}_2$
1.1
1.2
1.3
1.4
1.5
1.6
W [GeV]

Fig. 19

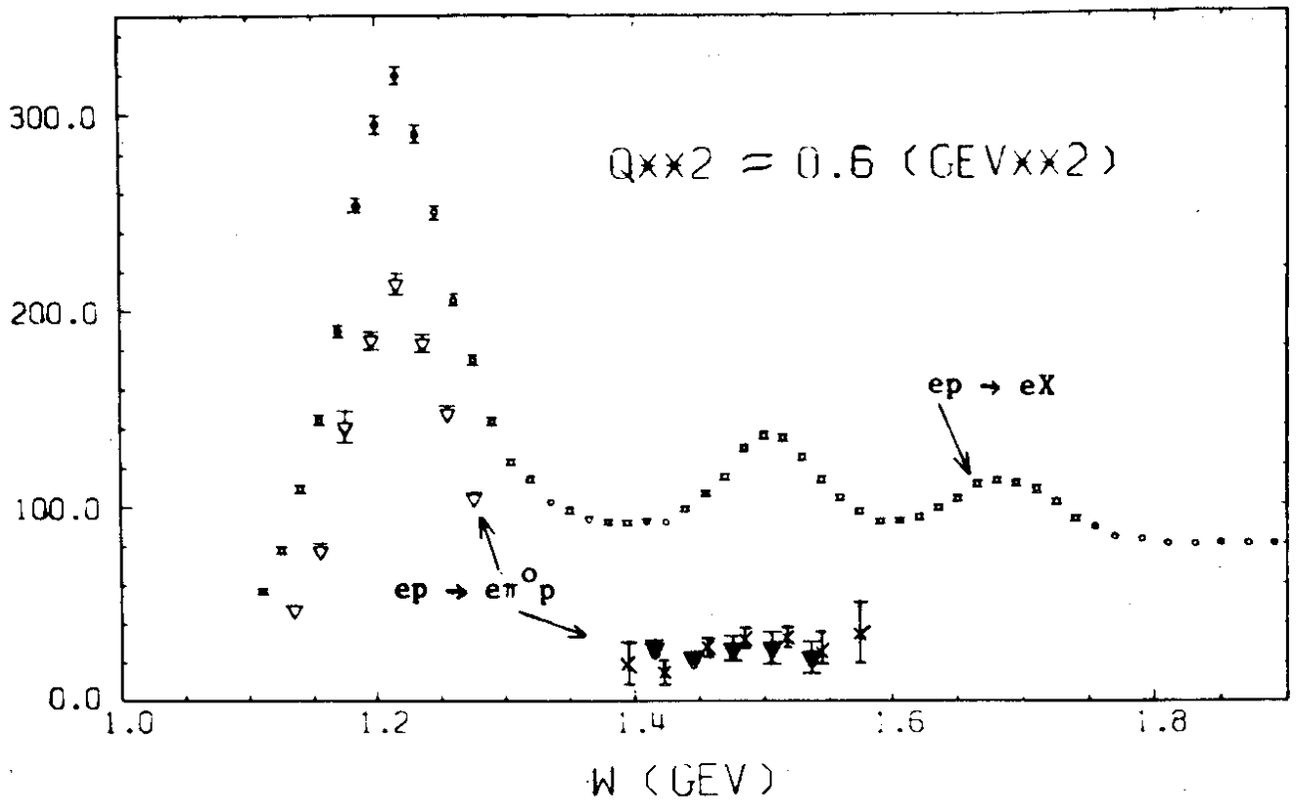
Q**2 = 0.6 (GEV**2)
ep → eX
ep → eπ°p
300.0
200.0
100.0
0.0
1.0
1.2
1.4
1.6
1.8
W (GEV)

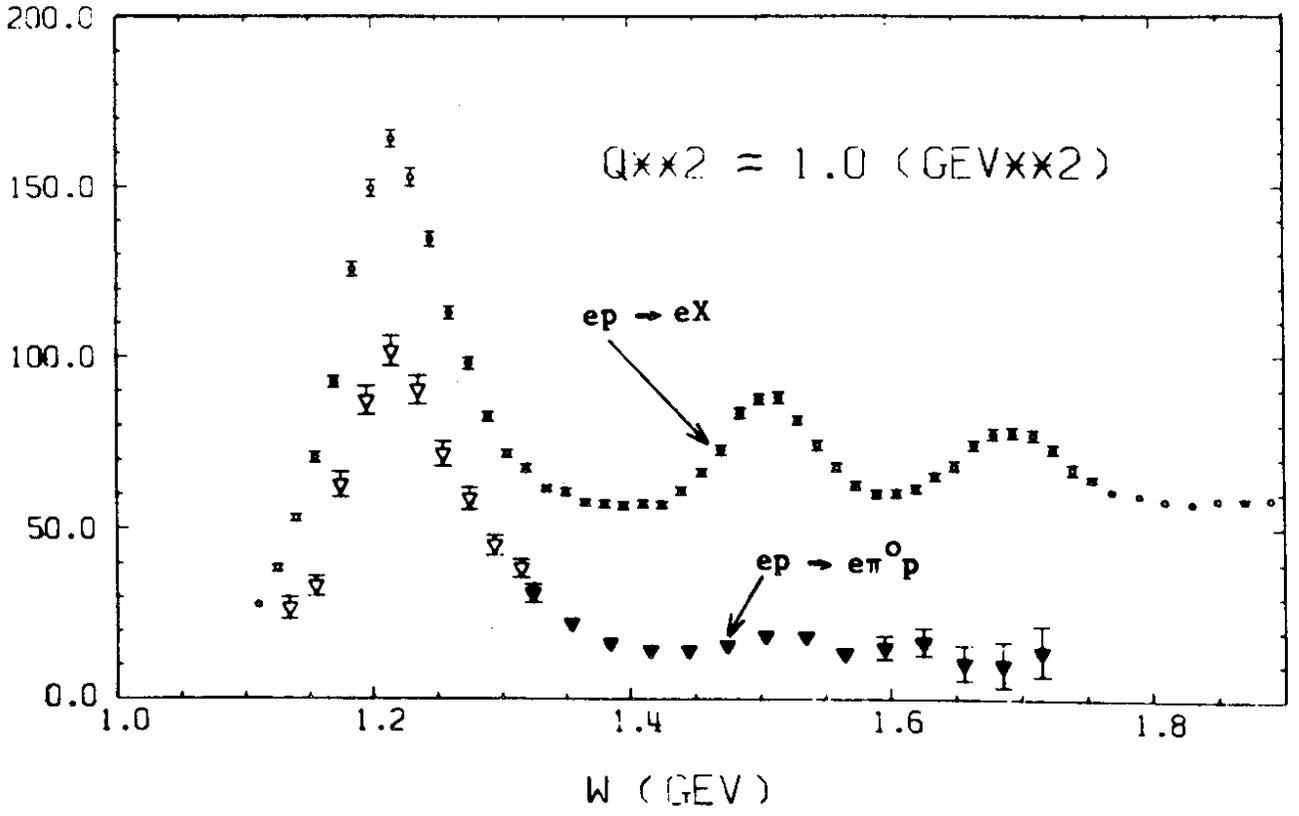
Q**2 = 1.0 (GEV**2)
ep → eX
ep → eπ°p
200.0
150.0
100.0
50.0
0.0
1.0
1.2
1.4
1.6
1.8
W (GEV)

Fig. 20

$\gamma_v p \longrightarrow \pi^+ n$

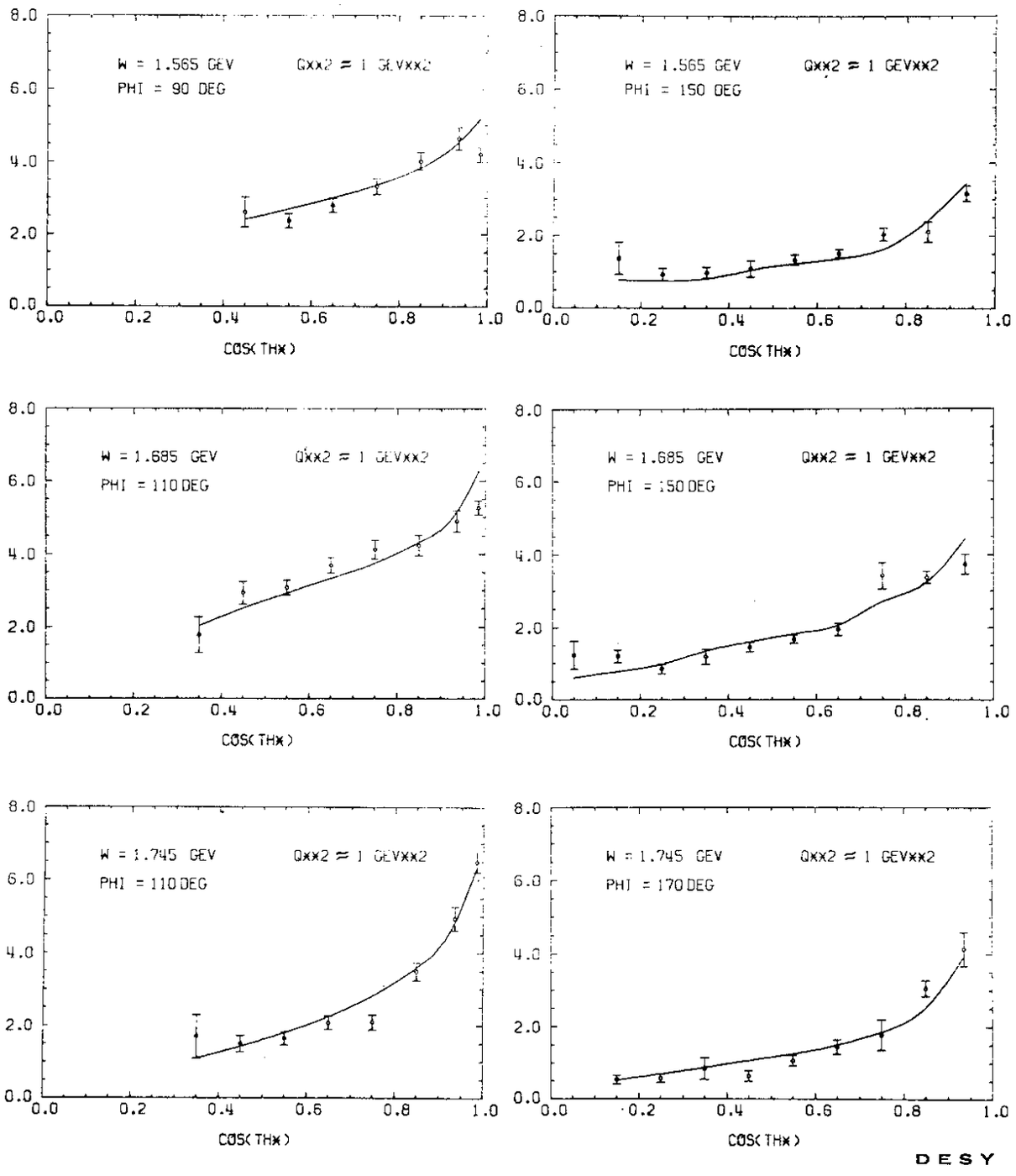

DESY

25094

Fig. 21

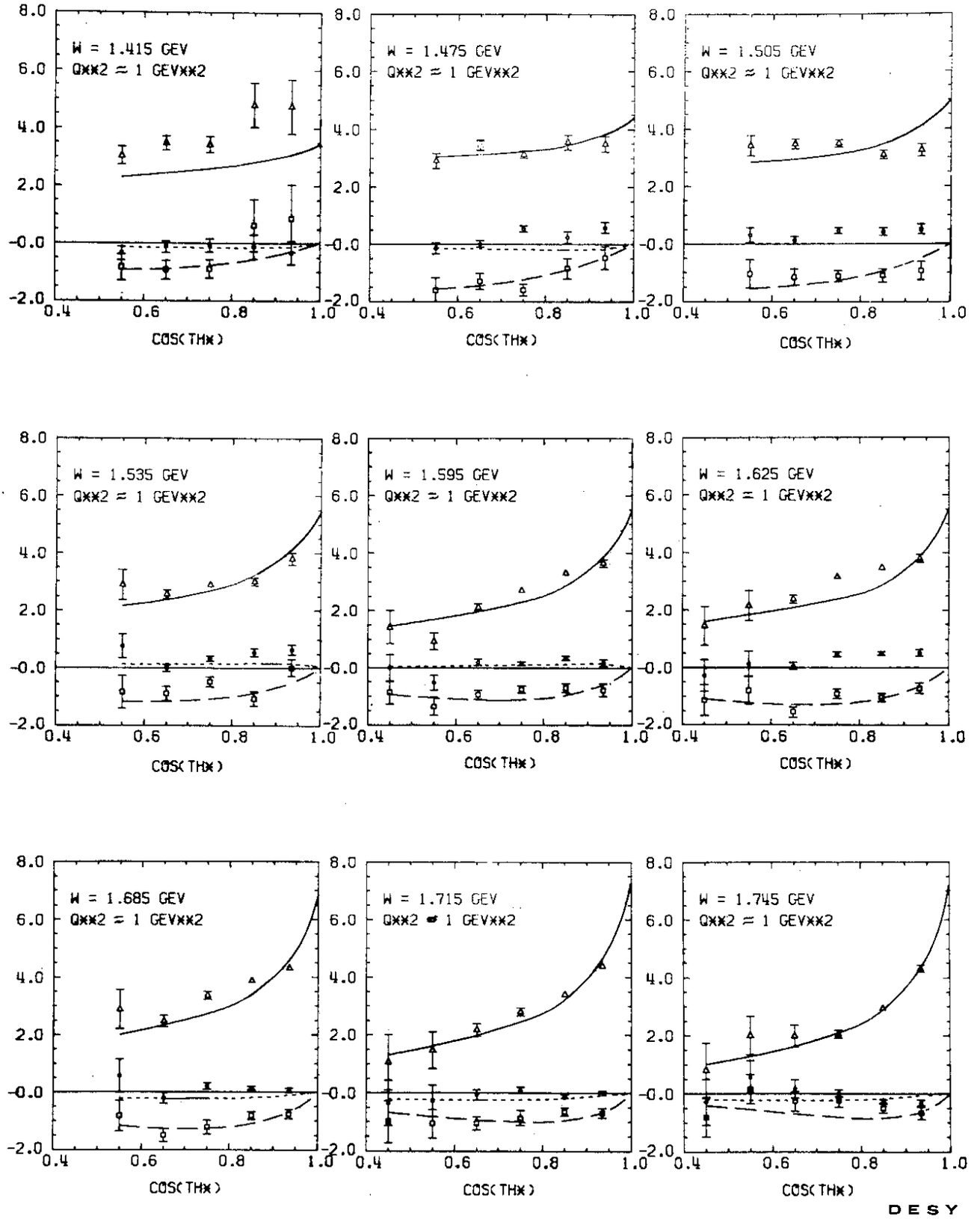
$\gamma_v p \rightarrow \pi^+ n$
W = 1.415 GEV
Q**2 = 1 GEV**2
W = 1.475 GEV
Q**2 = 1 GEV**2
W = 1.505 GEV
Q**2 = 1 GEV**2
W = 1.535 GEV
Q**2 = 1 GEV**2
W = 1.595 GEV
Q**2 = 1 GEV**2
W = 1.625 GEV
Q**2 = 1 GEV**2
W = 1.685 GEV
Q**2 = 1 GEV**2
W = 1.715 GEV
Q**2 = 1 GEV**2
W = 1.745 GEV
Q**2 = 1 GEV**2
COS(THE*)
DESY
25095

Fig. 22

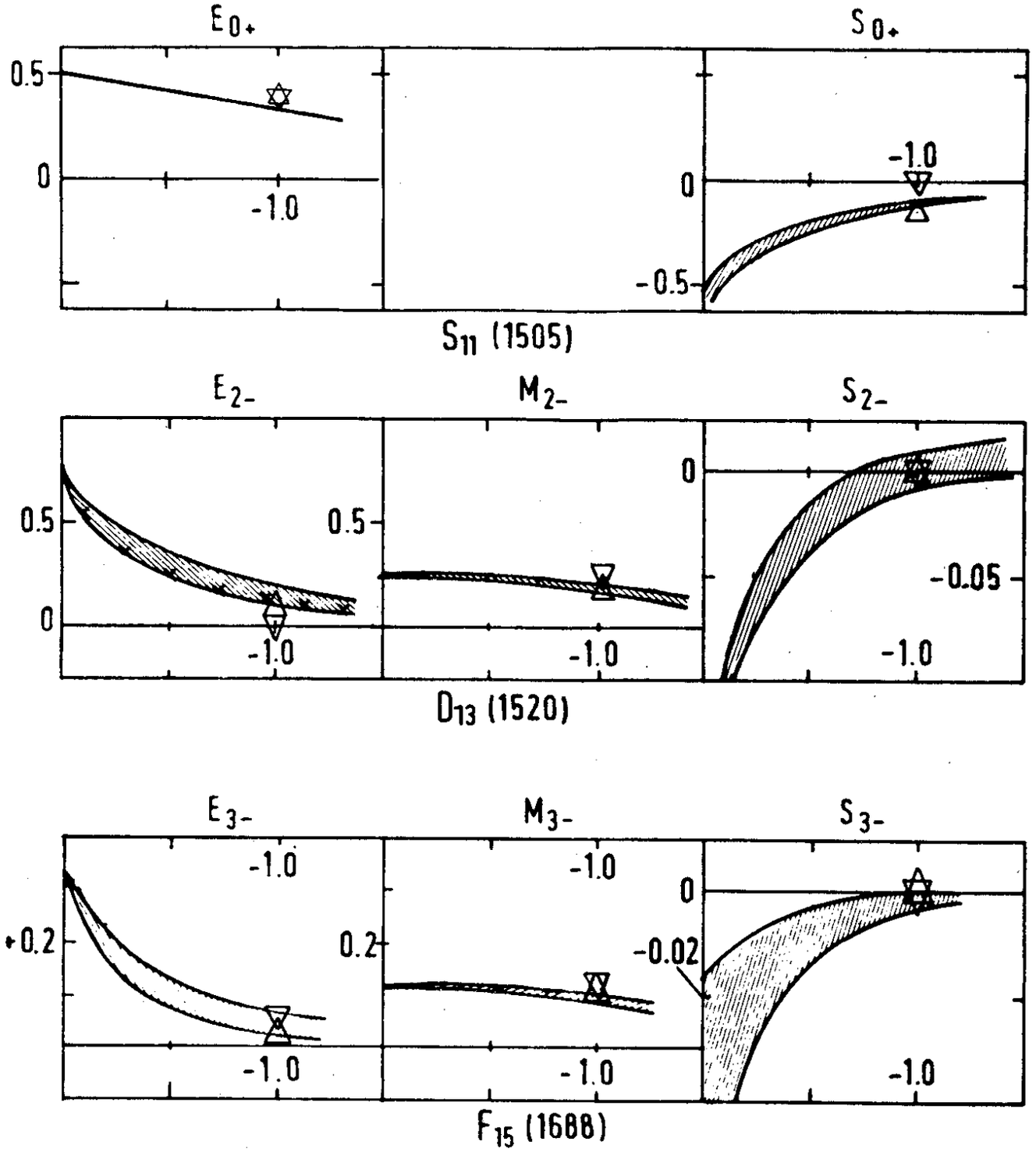
E0+
S0+
0.5
0
-1.0
0
-1.0
-0.5
S11 (1505)
E2-
M2-
S2-
0.5
0
0.5
0
-0.05
-1.0
-1.0
-1.0
D13 (1520)
E3-
M3-
S3-
-1.0
-1.0
0
+0.2
0.2
-0.02
-1.0
-1.0
-1.0
F15 (1688)
Q2(GeV)

Fig. 23

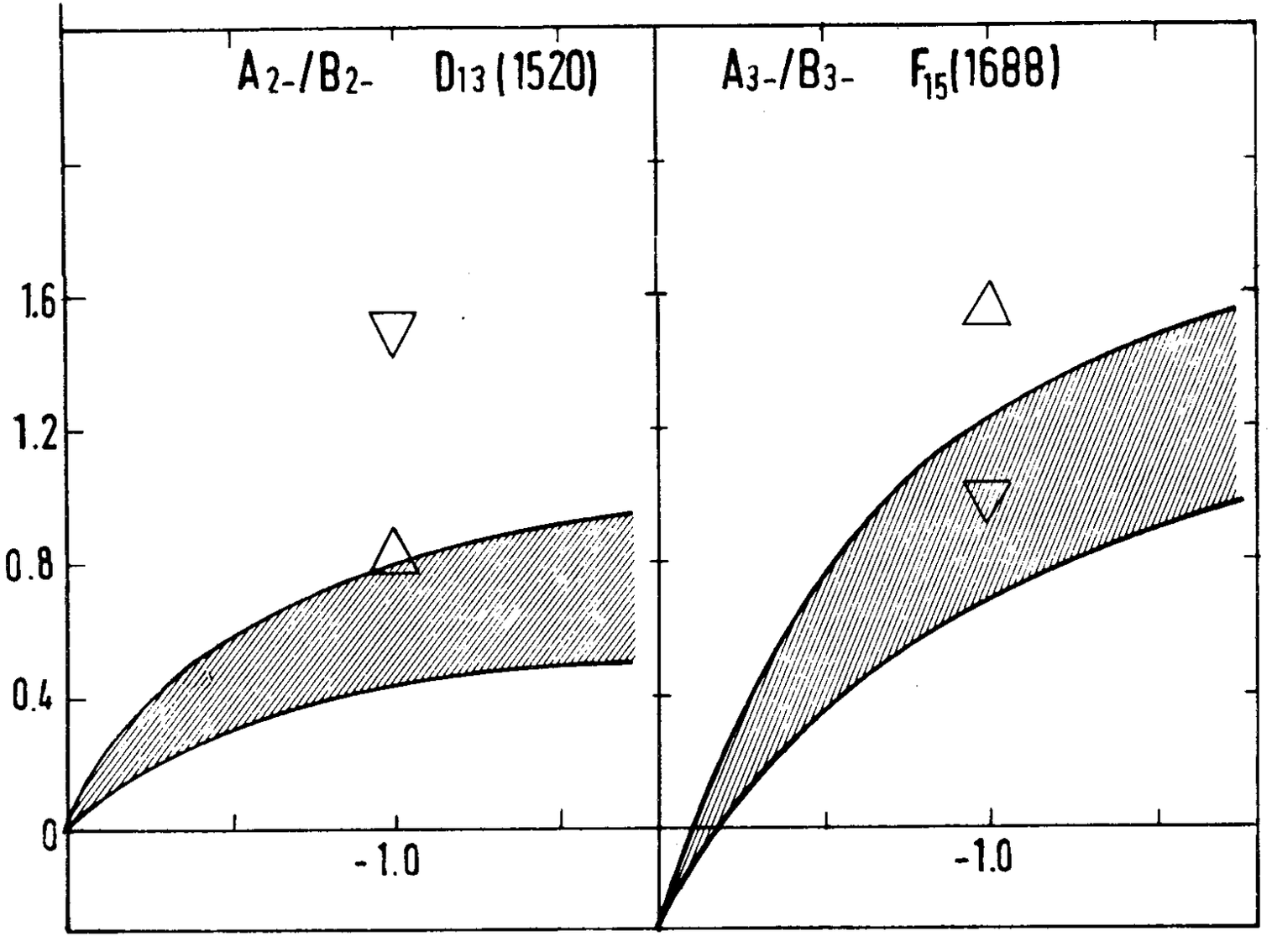

Fig. 24

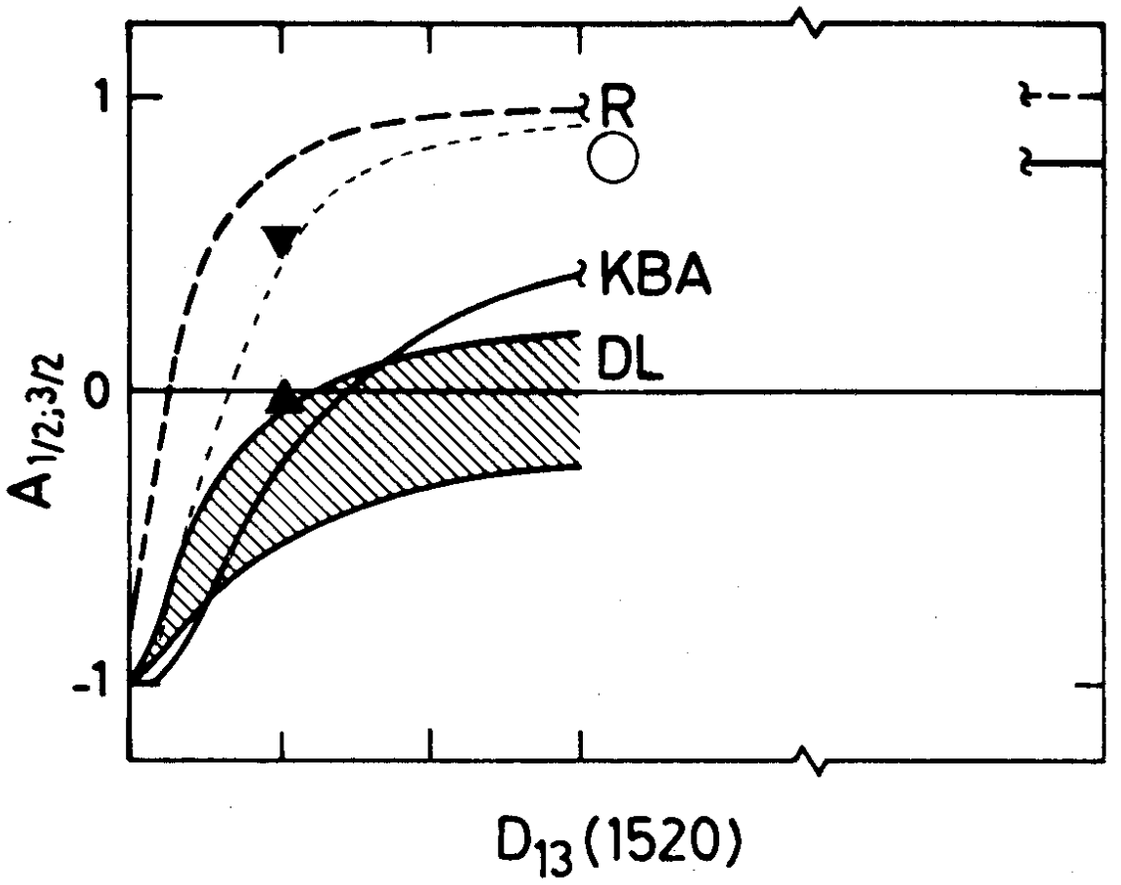
1
0
-1
$A_{1/2;3/2}$
R
KBA
DL
$D_{13}(1520)$

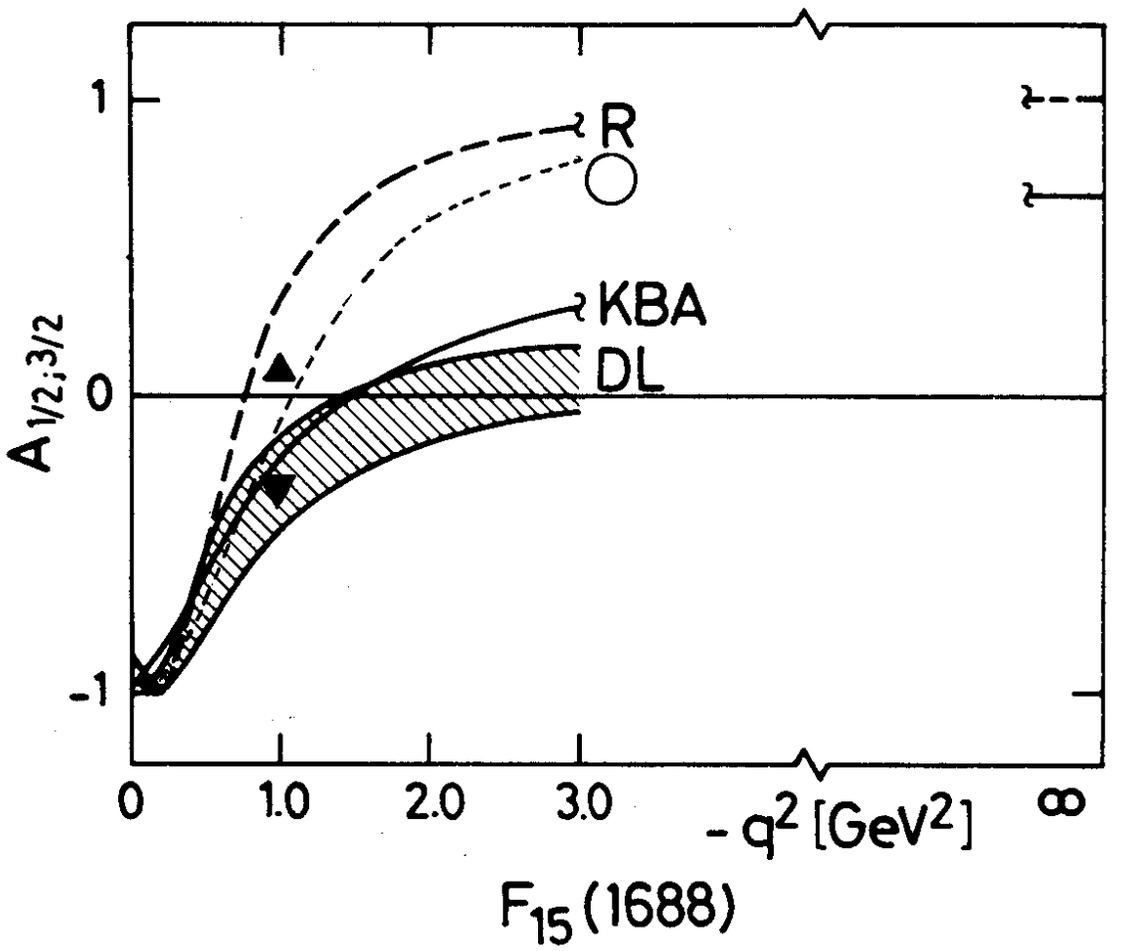
1
0
-1
$A_{1/2;3/2}$
R
KBA
DL
0
1.0
2.0
3.0
$-q^2$ [GeV^2]
∞
$F_{15}(1688)$

Fig. 25